AD-762 851

INVESTIGATIONS OF THE RELATIONS BETWEEN RESIDUAL STRAINS, FABRIC, FRACTURE, AND ULTRASONIC ATTENUATION AND VELOCITY IN ROCKS

Melvin Friedman

Texas A and M Research Foundation

Prepared for:

Bureau of Mines
Advanced Research Projects Agency

1 June 1973

a report [redacted]

from the Texas A&M
RESEARCH FOUNDATION
College Station, Texas

[redacted]

UNCLASSIFIED

Security Classification

DOCUMENT CONTROL DATA - R & D

(Security classification of title, body of abstract and indexing annotation must be entered when the overall report is classified)

1. ORIGINATING ACTIVITY (Corporate author)

Texas A&M Research Foundation
FE Box H, College Station, Texas 77843

2a. REPORT SECURITY CLASSIFICATION

UNCLASSIFIED

2b. GROUP

3. REPORT TITLE

INVESTIGATIONS OF THE RELATIONS BETWEEN RESIDUAL STRAINS, FABRIC, FRACTURE, AND ULTRASONIC ATTENUATION AND VELOCITY IN ROCKS

4. DESCRIPTIVE NOTES (Type of report and inclusive dates)

Final Report - May 2, 1972 - June 1, 1973

5. AUTHOR(S) (First name, middle initial, last name)

M. Friedman

6. REPORT DATE	7a. TOTAL NO OF PAGES	7b. NO. OF REFS
June 1, 1973	77	21

8a. CONTRACT OR GRANT NO

H0220062

b. PROJECT NO

ARPA Order No. 1579
Amend 3
Program Code 2F10

c.

d.

9a. ORIGINATOR'S REPORT NUMBER(S)

Project No. 861 - Final

9b. OTHER REPORT NO(S) (Any other numbers that may be assigned this report)

10. DISTRIBUTION STATEMENT

Distribution of this document is unlimited.

11. SUPPLEMENTARY NOTES

12. SPONSORING MILITARY ACTIVITY

Advanced Research Projects Agency

13. ABSTRACT

Residual strains, fabric, ultrasonic velocity and attenuation, and fracture anisotropy in blocks of Charcoal Granite, Sioux Quartzite, and Berea Sandstone are investigated to determine their causes and effects and the degree to which the attributes can be used to predict fracture anisotropy. Orientations of tensile fractures, induced by point loading oriented discs, are reliably predicted from ultrasonic data in all three rocks with the attenuation data reflecting some not sensitive to velocity. In the granite the fractures are compatible geometrically and probably genetically with the orientations and magnitudes of the residual strains as measured by X-ray diffraction analysis and with several aspects of the fabric. Fractures not parallel to the bedding in the quartzite and sandstone are compatible with residual strains measured by X-rays (quartzite) and with those detected by strain relief (sandstone). Ultrasonic data for these bedded rocks do not correlate with any of the fabric elements studied. The tendency for fractures to propagate along grain boundaries in these rocks suggests minute openings may exist at the boundaries that may influence the fracture and acoustic properties.

Strain relief results are inherently ambigous. Each time a new free surface is introduced the residual strains reorganize into a new state of internal equilibrium. The principal axes of the cumulative strain changes tend to be compressional normal to the free surface and extensional parallel to it. The relaxations at a given site are apparently controlled by the original stored strains in the test block (probably modified from those in the rock mass by sample collection), proximity to and shape of the free surfaces, and the size and shape of the test block. These factors preclude good correlations between strain-relief data and the other parameters studied herein, and may cause borehole gage determinations of in situ stress to be misinterpreted in rocks with relative large residual strain.

DD FORM 1 NOV 1473

UNCLASSIFIED

Security Classification

14 KEY WORDS	LINK A		LINK B		LINK C	
	ROLE	WT	ROLE	WT	ROLE	WT
attenuation						
fabric						
fracture anisotropy						
in situ stresses						
microfractures						
point loading						
prediction						
rapid excavation						
relative amplitude						
residual strain						
residual stress						
strain relief						
tensile fracture						
ultrasonics						
velocity						
X-ray diffractometry						

FINAL REPORT

on

INVESTIGATIONS OF THE RELATION BETWEEN RESIDUAL STRAINS, FABRIC, FRACTURE, AND ULTRASONIC ATTENUATION AND VELOCITY IN ROCKS

BY

Melvin Friedman
Principal Investigator

[713] 845-3251
Center for Tectonophysics
Texas A&M University

This Research Was Supported By The Advanced Research Projects Agency Of The Department of Defense And Was Monitored

by the

BUREAU OF MINES

Contract No. H0220062

Sponsored by
Advanced Research Projects Agency
ARPA Order No. 1579, Amend. No. 3
Program Code 2F10

Contract Date May 2, 1972 to June 1, 1973

Contract Amount $26,886

Texas A&M Research Foundation
FE Box 14
College Station, Texas 77843

INVESTIGATIONS OF THE RELATIONS AMONG RESIDUAL STRAINS, FABRIC, FRACTURE AND ULTRASONIC ATTENUATION AND VELOCITY IN ROCKS

by

M. Friedman
Center for Tectonophysics
Texas A&M University
College Station, Texas 77843

SUMMARY

Efficient rapid underground excavation requires the development of geological and geophysical techniques for determining the quality of the rock mass prior to excavation and during excavation by probing immediately ahead of the working face. Ideally the engineer primarily needs to know breaking strengths of the rocks, the abundance and orientation of macroscopic and microscopic defects, rock anisotropies, and the in situ state of stress in addition to lithology, ground and water conditions. Work on sonic investigation of rocks by the U. S. Bureau of Mines (Refs. 1-3) shows that attenuation and velocity fields correlate with, and therefore, can be used to map, at least qualitatively, the rock fabric, fracture anisotropy and unconfined breaking strength. If the sonic method also correlates with the residual and in situ states of stress then the possibility exists that sonic probing of the rock mass may yield simultaneously much of the pertinent information required to engineer the rapid underground excavation.

The purpose of this study is to determine the nature of the correlation bewteen residual strains (stresses) in rocks as measured by strain-relief and X-ray diffraction techniques, rock fabric, fracture anisotropy and ultrasonic attenuation and velocity fields. If a positive correlation exists among these phenomena, as initial study suggests, then this work could serve as the basis for the development of a practical approach to the combined measurement of nearly all intrinsic factors known to influence fracture anisotropy in rock, namely: ultrasonics.

Specifically the relations among the ultrasonic data, residual strains, fracture and fabric are studied in three blocks of rock: Charcoal Granite, Sioux Quartzite, and Berea Sandstone. These are being used because (a) the U. S. Bureau of Mines, Twin Cities Mining Research Center could supply the blocks (about 0.02 m^3 each) and the corresponding ultrasonic data, (b) the rocks contain quartz from which residual strains can be determined by X-ray diffractometry, and (c) the textures and compositions of these rocks cover much of the spectrum of "hard" rocks commonly encountered in engineering practice. There was no way of knowing beforehand whether the blocks would contain measureable residual strains. For each block the residual strains are measured by both strain relief and X-ray methods (Refs. 5 and 7). For the strain-relief work an array of thirteen 45^{o}-rosette gages are mounted on each block and those of the XY surface are sequentially and concentrically overcored and undercored by 15-cm, 10-cm, and 5-cm diameter drill bits. The resulting strain changes at each rosette are recorded with a Vishay, Model P-350A strain indicator purchased for this work. The relative tensile fracture strength and the existence of possible fracture anisotropies are determined by point loading three sets of mutually perpendicular discs cored from each block. Microfractures, cleavage planes, exsolution lamellae, deformation lamellae, grain boundaries, and long grain axes , fabric elements that could possibly serve as defects or flaws and influence fracture anisotropy or the ultrasonic data, are studied in thin section with standard universal stage techniques.

The orientations of tensile fractures, induced by point loading, are reliably predicted from ultrasonic data, particularly the relative amplitudes (attenuation), in all three rocks. In the granite the fractures are compatible geometrically and probably genetically with the orientations and magnitudes of the residual strain as measured by X-ray analysis and with several aspects of the fabric. For the bedded quartzite and sandstone, fractures not parallel to bedding are compatible with residual strains measured by X-rays (quartzite) and with those detected by strain relief (sandstone). In the quartzite and sandstone the ultrasonic data do not correlate with any of the fabric elements studied. The tendency for fractures to propagate along grain boundaries in these rocks suggests minute openings or flaws exist along the boundaries and which may influence the fracture and acoustic properties.

Strain relief results are inherently ambiguous. Each time a new free surface in introduced the residual strains reorganize into a new state of internal equilibrium. The principal axes of the strain changes generally are compressional normal to the free surface and extensional parallel to it. Further, strain changes often vary in orientation, magnitude, and/or sign (compression or extension) from one concentric overcore to the next. In general the relaxations are apparently controlled by the original stored strains in the test block (probably modified from those in the rock mass by sample collection), proximity to and shape of free surfaces, and the size and shape of the test block. These factors preclude good correlations between strain-relief data and the other parameters studied herein, and may cause borehole gage determinations of the in situ state of stress to be misinterpreted in rocks for which the residual strain component is relatively large.

No patentable devices are involved in this work.

ACKNOWLEDGMENTS

The blocks of Charcoal Granite, Sioux Quartzite, and Berea Sandstone and the matching ultrasonic data are supplied by the U.S. Bureau of Mines, Twin Cities Mining Research Center. The writer is particularly indebted to Mr. T. R. Bur of the Twin Cities Research Center for facilitating this work and for supplying and interpreting the ultrasonic data. Measurements of residual elastic strains by strain-relief and X-ray diffractometry, the fabric analyses, and the detection of fracture anisotropies through point loading tests were done in the laboratories of the Center for Tectonophysics, College of Geosciences, Texas A&M University. For their help in obtaining these data thanks go to G. H. Alani, T. L. Blanton III, R. E. Conrad, J. C. Coyne, L. D. Dyke, and J. N. Magouirk. This research was supported by the Advanced Research Projects Agency of the Department of Defense and was monitored by the U. S. Bureau of Mines under Contract No. H0220062. No patentable devices are involved in this work.

PREVIOUS WORK

Workers at the Twin Cities Laboratory have developed an ultrasonic method for mapping attenuation and velocity fields in rocks, and they have correlated these with rock fabric, fracture anisotropy, and unconfined breaking strength (Refs. 1-3). Workers at the Center for Tectonophysics have studied residual strains by the strain-relief techniques in the laboratory and in the field, have developed an X-ray method for measuring the three-dimensional state of residual strain, and have demonstrated that the residual strains (prestresses) can influence the orientations of induced fractures and the breaking strengths of rocks under confining pressures to 1500 bars (Refs. 4-7). The concepts, techniques and procedures for the ultrasonic and fabric work need no further

elaboration here, but certain aspects of residual strain need elaboration.

Residual strains. A comprehensive review of residual elastic strain in rocks and of the different measuring techniques is given by Friedman (Refs. 4, 5, and 61) and by Hall and Hoskins (Ref. 8). Residual strains (stresses) are potentially recoverable elastic distortions of constituent crystals or grains that satisfy internal equilibrium conditions and that exist in a given volume of rock with no external loads across its boundaries (Refs. 9, 10). It is helpful to think of residual strains as composed of two parts: (1) crystal distortions, reflecting previous external loads, that are locked in the aggregate, called the locked-in strains (or corresponding stresses), and (2) those that constrain them, called the locking strains (or stresses). For equilibrium to exist the sum of the forces causing the two must equal zero. Neither the locked-in stresses nor the locking stresses need be transmitted across the whole of any arbitrary cross-sectional area through a rock. In detail, a small portion of the area may carry the locking stresses while a complementary larger area may carry the locked-in stresses or vice versa. Similarly the two components of residual stress need not be equally distributed volumetrically. Although static equilibrium demands that the stresses balance the corresponding locking and locked-in strains need not. For example, if the locked-in strains are carried by elements of high stiffness and the locking strains by relatively less stiff elements then the locking strains would be larger than the locked-in strains even though the forces causing the two are equal and opposite.

The concept of locked-in and locking stresses provides at least a qualitative view of certain phenomena reported herein and elsewhere in

literature. For example, when the boundaries of a rock containing residual stresses are changed by fracture, saw cuts, or by over-or undercoring, free surfaces are introduced, locking stresses are broken, and there is corresponding relaxation of the locked-in stresses as a new state of equilibrium is established. During this process strains due to the relaxation in one region of the block can be transmitted to other regions. Strain gages mounted on the block record some combination of the relaxed locking and locked-in strains as well as the redistribution of strains transferred within the body. The exact proportions of these components in the resulting data are functions of the size, location, and elastic moduli of the domains carrying the locking and locked-in strains as well as the relative magnitudes of the relaxations of the two strain components.

The quantity measured either by strain-relief or X-ray diffraction is actually a displacement, a length, which when subtracted from an original length and divided by the original length yields a strain. It is customary either to express the result as a strain or as a stress. Precise expression of residual strains as stresses is difficult. One would need to know the distribution and magnitudes of locking and locked-in strains, the combination of the two that relax (strain relief) or that are detected by the X-ray method, and the elastic moduli of the rock elements serving as the locking and locked-in components. Use of moduli for the rock as a whole, which is the general practice in strain relief measurements, yields only an approximate conversion to stress.

From the concept of residual strain outlined above it follows that the residual strains (states of residual strain, principal strain axes, etc.) reported in this paper and in the literature represent only some observed combination of locking and locked-in strains. They might best be called apparent or observed residual strains.

Through previous investigations (Refs. 4-7) certain facts are known about

the observed residual stresses as determined by X-ray diffractometry.

1. Magnitudes can be large, differential stresses between 300 and 400 bars have been found in quartzites, sandstones, and granites.

2. They can be related geometrically to large-scale folds.

3. They can be related to local sliding surfaces.

4. They relax when grains are freed from constraints of nearest neighbors.

5. They relax all or in part within $\pm$ 4 mm of a fracture surface.[1]

6. They control the orientations of fractures induced under certain conditions of loading.

7. They help produce strength anisotropy in some rocks.

The detailed laboratory study of residual strains in a block of Barre Granite by Nichols (Ref. 11) is noteworthy because the strain-relief procedures employed here are patterned after Nichols' approach. He installed thirty-six 45°-rosette foil gages in three arrays on three faces of the block, and he sequentially and concentrically overcored each array with 5-cm, 10-cm, and 15-cm diameter diamond drill bits. The response of the rock is complex, but in general the rock initially contracts along radial directions and either contracts or expands along circumferential directions relative to the series of concentric overcores. Each overcoring results in an additional change in strain at each rosette location--even those distant from the new free surfaces. Gages located nearest these newly created free surfaces give the largest strain changes. After the top surface has been completely cored, the whole external rind of the block extends, and the strains change with time. For example, on the bottom of the block the gages record an initial contraction as the top is overcored, but then extend back to the initial zero state in about 48 hours. Anomalously large expansions at a few gage locations are attributed to the opening of microfractures or grain boundaries. The fact that at many gage locations the rock contracts in all directions parallel to the surface

[1] Relaxations upon strain relief are clearly over much larger distances.

indicates that (1) fracture opening cannot be the mechanism of relaxation, and (2) at least the outer rind of the block was initially in a state of tensile residual stress prior to the overcoring.

Also important to the present study is the fact that the principal axes of residual strain determined by the X-ray method are in excellent agreement with Nichols' secondary principal strains measured at the center of the top surface of his block of Barre Granite (Ref. 7, Figure 4). The corresponding axes are just 17° apart; and whereas Nichols measured contractions upon strain relaxation the X-rays detected corresponding extensions still stored in the rock.

Residual and in situ stresses. The in situ state of elastic strain (stress) consists of two components: the strains caused by currently applied loads and the residual strains. If there are no external loads across the boundaries of a rock, as in the laboratory or in special field situations, the potentially recoverable in situ strains are the residual strains. These relate to the paleotectonic, paleotopographic, and thermal and chemical histories of the rock. If a rock free of residual strain is currently under loads caused by present topography, present tectonics, or the works of man, then the in situ strains are termed applied strains. In the general field or subsurface condition, applied strains and loads are superposed on residual strains and stresses (Ref. 12). In this study the ultrasonic data are determined for spheres of rock at atomospheric pressure; hence it is only the residual strains that are important here.

X-ray diffraction method. Many of the facts concerning residual strains have been obtained with the X-ray diffraction method. This technique yields a special measure of the residual strains (Ref. 7), and are given here for the convenience of the reader. The X-ray technique itself will not be reviewed here (see Friedman, Ref. 4).

(a) The X-ray measurements are made on small chips of rocks with no external loads across their boundaries so that the strains calculated by com-

paring observed and strain-free d spacings (i.e., change in length divided by original length) are residual.

(b) The technique permits measurement of the residual strain in a particular mineral species in a specific small region and along a given direction in the body. Data are available for quartz (d spacing for $\{32\bar{5}4\}$) in a variety of quartz-rich rocks. As a first approximation the elastic strains are converted to stresses by use of the elastic stiffness normal to $\{32\bar{5}4\}$ in quartz, 0.89×10^6 bars (compliances for quartz supplied by J. M. Christie, Department of Geology, UCLA, personal communication, 1966). The stiffness normal to $\{32\bar{5}4\}$ is about halfway between the maximum and minimum stiffnesses for quartz. For a condition of homogeneous strain use of the d-spacing for other $\{hk\bar{i}l\}$ planes with a stiffness different from that for $\{32\bar{5}4\}$ would yield a strain of different magnitude, but the orientations of computed principal strain axes would be the same. Similarly, the stresses calculated using the appropriate stiffnesses would be the same as for $\{32\bar{5}4\}$.

(c) The strain calculated from the observed d-spacing changes is some unknown combination of the locked-in and locking strains. The intensity of the diffracted X-ray beam, and therefore the peak 2θ position of the diffraction profile, from which d is measured, depends on the volume of material satisfying the Bragg condition. In a quartz cemented sandstone, for example, the volumetric ratio of grains to cement is always > 1. Thus a given diffraction peak might contain diffracted quanta from both cement and grains, but the 2θ position of the peak (from which d and the strain are calculated) will be biased, at least statistically, by the diffraction events from the grains. In general, therefore, strain calculated from the observed diffraction

profile will be biased by the strain in the most voluminous rock elements in the diffracting orientation.

(d) The technique yields an assessment of the degree of homogeneity of the strain fields. Extreme heterogeneity of strain between regions carrying locking and locked-in strains is logicably to be expected. Moreover, the strain fields within grains of a rock under load (and locked in) are complex. Thus even if the diffracted events are biased toward the grains, the resulting calculated strains Z tend to give an "average" for the diffracting material. It is an experimental fact, however, that similar strains along a given direction in space often are detected at different areas of irradiation, and that the average strains for different direction in space often are compatible (see e, below). These data suggest that in some rocks there is a reasonable degree of homogeneity of the measured residual strains.

(e) The technique provides a three-dimensional determination of the directions and magnitudes of the "average" principal strains. The X-ray method is designed to provide normal strains along more directions in space than are needed to calculate the strain ellipsoid. Accordingly six sets of principal strain axes are calculated (Eigenvalue solution) each from a different set of strain components. As mentioned in (d) a measure of the degree of homogeneity of the strains is afforded by the degree of agreement observed among corresponding principal axes from the six sets of axes.

Residual strains and ultrasonic data. At least a geometric if not a genetic correlation between residual strains, fabric, and ultrasonic data has been demonstrated for Barre Granite (Ref. 7). Ultrasonic velocity and attenuation data were published by Bur and others (Ref. 2) and the corresponding fabric

data by Willard and McWilliams (Ref. 3). Residual strains were determined by means of X-ray method from two oriented discs from the same block of the granite as utilized by the above workers. The X-ray data indicate the residual strains are homogeneously distributed in the rock at least over the scale of the two discs (each 5 cm in diameter by 1 cm thick). The average magnitudes of the principal strains equate to a large differential stress ($\sigma_1 - \sigma_3$) of about 340 bars. The orientations of the principal strain axes are each within 20° of the principal axes of the fields of relative amplitude and velocity determined by ultrasonic measurements. Moreover, the greatest, intermediate, and least principal elongations of the state of residual strain correlate with the low (L), and medium (M), and high (H) axes of the ultrasonic symmetry fields. In addition, the "rift" of the rocks parallels the H-M symmetry plane which corresponds to the plane containing the least and intermediate principal elongations of the state of residual strain; and the tensile breaking strength is minimal parallel to L and the greatest principal elongation (Ref. 3). The directions of "rift" and minimum tensile strength agree with predictions from knowledge of the prestrain (Ref. 6). Excellent agreement thus exists between the X-ray, ultrasonic, and strength testing data for the Barre Granite.

METHOD OF STUDY

The procedure for study of each block of rock (Charcoal Granite, Sioux Quartzite, and Berea Sandstone) is as follows:

1. Each block (approximately 25 cm on a side) is shaped into a rectangular parallelopiped by sawing and polishing. Orientation coordinates X, Y, and Z are established relative to markings supplied by the Twin Cities Research Laboratory, and are the common frame of reference throughout the study.

2. 45°-rosette foil resistance strain gages are mounted at position 1 on the XY surface and at the lower left-hand corner of the YZ surface of the

block (Figure 1). The latter is overcored with a 5-cm diameter drill bit and the relaxation of residual strains, if any, are recorded at both gages. This procedure is necessary to determine if the block contains any residual strains detectable by strain relief and to provide samples (from the overcore) for X-ray study of residual strain and for three mutually perpendicular thin sections for fabric analysis.

3. The "average" state of residual strain is determined by X-ray diffractometry.

4. Any macrofractures or other planes or zones of mechanical discontinuity that intersect the surfaces of the block are observed and recorded.

5. The complete array of 45°-rosette gages is installed on the XY, YZ, $\bar{Y}Z$, and $\bar{X}Z$ faces of the block (Figure 1). The gages are spaced so that they will not be damaged upon drilling with 15-cm, 10-cm, and 5-cm diameter drill bits that each produce a kerf of 5 mm. The individual gages of each rosette are 2 mm by 4 mm. The gages are connected through an internally balanced switching unit to a Vishay, Model P-350A, strain indicator (Figure 2). Temperature compensation is achieved through a "dummy" gage that is kept in the same environment as the active gages. All gages are monitored for apparent changes possibly inherent in technique, i.e., changes caused by temperature and moisture variations, and by disconnecting and remaking the soldered electrical connections which must be done for each overcore. Apparent strains introduced by these procedures average 3×10^{-6} with a standard deviation of 4×10^{-6}. Using the confidence level of $\pm$ 2 standard deviation, therefore, strain changes in excess of $\pm\ 10 \times 10^{-6}$ are significant.

6. The gage array on the XY surface is overcored with a 15-cm diameter drill bit to a depth of 9 cm (Sioux Quartzite) or 15 cm (Berea Sandstone). Strain changes at each rosette are recorded as soon as all electrical connections are remade. The gages are monitored at intervals until no further significant strain changes are detected. Record of the strain changes at each gage for each overcoring is kept throughout the experiment. Secondary principal strains E_1 and E_2 are

calculated from each rosette. This record for gage 1 is given as an example in Table 2.

7. The XY surface is then concentrically overcored with the 10-cm diameter drill bit to the same depth as the 15-cm overcore, and all gages are monitored as in (6).

8. The XY surface is then overcored with the 5-cm diameter drill bit to the same depth, and all gages are monitored as in (6).

9. Three sets of mutually perpendicular oriented discs (2.5 cm) in diameter by about 1.3 cm thick) are then prepared from the block for point loading. This test provides information of any fracture anisotropy that might exist (Ref. 6) and on the relative tensile strengths (Ref. 12).

10. Residual strains are re-measured by X-ray diffractometry immediately under gages No. 1 on the XY surface (Figure 1).

11. The surface of the block under the gages are re-examined for the development of fractures possibly produced by strain relief.

12. Fabric data are determined from thin section study.

13. All data are analyzed and correlated.

OBSERVATIONAL RESULTS

Charcoal Granite

Composition. The Charcoal Granite, St. Cloud, Minnesota (also known as the St. Cloud Gray Granodiorite), is a massive, dark brown to dark gray granodiorite consisting of 38% plagioclase feldspar, 26% orthoclase, 21% quartz, 12% hornblende, and 3% biotite. The feldspars are somewhat altered and contain abundant exsolution lamellae. Healed microfractures are conspicuous in the quartz and feldspar. Grain size range is from < 0.1 to 10 mm and averages about 1 mm. No conspicuous macrofractures occur at the surfaces of the block.

Residual Strains. Following the procedures in Step 2 (above) initial overcoring of the rosette mounted on the lower left corner of the YZ surface produced essentially no strain relaxation as detected by this gage or by rosette No. 1 (Figure 1). Strain changes at both rosettes are all < 20×10^{-6}. Rosette No. 11 is mounted and overcored, and again the relaxed strains at

rosettes 11 and 1 are < 20×10^{-6}. Further strain relief work (Steps 5-8) is suspended.

Specimens for X-ray study of the residual strains were prepared from the initial overcore, and the residual strains in the quartz of the rock were determined after Friedman (Ref. 4). The resulting six sets of principal strain axes are tightly grouped in space (Figure 3a) indicating the strains in the quartz are statistically homogeneous. The strains are small with the greatest principal elongation equal to 20×10^{-6} (extensions are positive), and the intermediate and least elongations equal to -35×10^{-6} and -65×10^{-6}, respectively.

Fracture Anisotropy. Three mutually perpendicular sets of oriented discs (2.54 cm diameter and about 1.4 cm thick) were prepared for point-loading tests designed to detect fracture anisotropy and relative tensile strength anisotropy (Ref. 6). Each disc is loaded, unconfined, between opposed ball bearings until it fails by the development of one or more tensile fractures. The loads are applied at uncontrolled, but not widely varying, rates with a Blackhawk ram; the load at failure ($\pm$ 5 psi) is recorded on a Heise gauge equipped with stop valve. After each set of oriented discs is loaded to failure the azimuths of the induced tensile fractures are measured along the radius of each disc relative to the coordinate axes. The azimuth of diametral fractures is measured separately along each opposing radius, and if the azimuths differ by 5° or more two fractures are counted. A plot of fracture azimuths for each set of similarly oriented discs (Figures 3b, c, and d) provides a measure of the fracture anisotropy. Data for the discs of Charcoal Granite are listed in Table 1. No significant strength anisotropy is found for the three directions of point-loading. The orientations of the induced tensile fractures (their azimuths relative to coordinates in the plane of each disc) are widely divergent in all three sets of discs, but there are statistically

significant groupings of fractures in two sets of discs. Both indicate a strong tendency to fracture essentially parallel to the XY plane.

Fabric. Planar fabric elements are studied that might be considered mechanical defects in the rock, and therefore, capable of influencing fracture or the ultrasonic data. These include long grain boundaries of feldspars, (0001) cleavages of biotite crystals, healed microfractures primarily in quartz and feldspar, exsolution lamellae and (010) cleavages in the feldspars, and albite and microcline twin lamellae.

The azimuths of the traces of long grain boundaries are somewhat preferrentially oriented in each of the three mutually perpendicular thin sections cut from the block (Figures 3e, f, and g). The orientation is strongest in the thin section parallel to the XZ plane (Figure 3f) where the grain boundaries are subparallel to the XY plane. There is a fair degree of correlation between the orientations of the long grain boundaries and those of the induced tensile fractures (compare Figure 3b and f, c and g, d and e).

Biotite cleavages are randomly oriented (Figure 4a), as are the (010) cleavage planes of the feldspars, and the feldspar twin lamellae (Figure 4b-d). Microfractures and exsolution lamellae, on the other hand, are preferrentially concentrated subparallel to the XY plane (Figure 4b and c). These elements are randomly oriented in the thin section parallel to the XY plane (Figure 4d). Thus the orientation trends of the microfractures and exsolution lamellae follow those of the induced tensile fractures.

Transgranular-Intergranular Fracture. Twenty-two tensile fractures (each about 1.3 cm long) formed in the point loading of ten discs are studied in thin section to determine the path of the fracture through the rock. For each fracture the distance increments within grains (transgranular)

and along grain boundaries (intergranular) are measured in a thin section cut perpendicular to the fracture surface. Willard and McWilliams (Ref. 14) found that the transgranular/intergranular ratio, (T/I), weighted for the abundance of the constituent minerals, is inversely proportional to loading rate for the Charcoal Granite. Unweighted T/I ratios for the twenty-two fractures studied here range from1.7 to 24 and average 5.88. Thus fracturing within grains is almost six times more frequent than along grain boundaries. It follows that fabric elements internal to the grains rather than the grain boundaries are more apt to control fracture orientation in this rock.

Ultrasonic Data. The average velocity and attenuation fields, determine from four to five spheres (Ref. 2), are shown in Figure 5. For the Charcoal Granite the velocity field (Figure 5a) is nearly axially symmetric about the Z coordinates axis, the axis of minimum velocity (between 4.7 and 4.8 km/sec). Velocities parallel to the XY plane are nearly the same (5.05 to 5.10 km/sec) with a maximum subparallel to Y. The average velocity is well below that of a relatively unfractured granodiorite. Thus the rock can be expected to have abundant microfractures. The velocity pattern suggests a strong set of microfractures perpendicular to the Z axis with a possible weak system perpendicular to the X axis.

Attenuation symmetry is similar to the velocity symmetry. The former also suggests a strong set of microfractures nearly perpendicular to the Z axis. The good signal in the Y direction and poor signal in the X direction suggest a second set of microfractures (or similar defects) with poles in the X direction and planes parallel to the Y axis.

Sioux Quartzite

Description. The block of low porosity, pinkish Sioux Quartzite (26.3 cm x 28.5 cm x 23.0 cm) exhibits conspicuous bedding oriented parallel to the

XY surface (Figure 1). The upper half of the block is cross-bedded, and two macrofractures occur parallel to bedding and about 5 cm apart in the lower half. The block has not lost cohesion across these fractures. On the top XY surface of the block where the array of ten rosette gages are mounted the mean grain size is about 0.2 mm, much smaller than the individual gages. No visible fracture occurs on the top surface or under gages 11-13.

Residual Strains: Strain-Relief Data. The history of the relaxation of the residual strains is complex and best presented following the sequence of overcoring. Upon initial test overcoring, the rosette on the YZ surface (Figure 1) and rosette 1 stabilized after 150 hours, i.e., no longer varied between readings by 10×10^{-6} (see Table 2). During this time the magnitudes but not the directions of the calculated secondary principal strain axes changed. The YZ gage initially recorded a greatest elongation (E_1) of 100×10^{-6} and a least elongation (E_2) of -190×10^{-6} (compression is negative); final values are $E_1 = 115$ and $E_2 = -130$. (Henceforth it is to be understood that strains are $\times 10^{-6}$). Initial strains at rosette 1 were $E_1 = 180$ and $E_2 = -100$, final values are $E_1 = 150$ and $E_2 = -110$. The magnitudes, sense, and orientation of these final strains are illustrated in Figure 6a and listed in Table 2. At this time rosettes 2 through 13 were not installed. The strains at rosette 1, which show E_1 oriented parallel to the X-45 direction (Figure 6a) indicate the recovery of a locked in compressive strain in this direction and vice versa for E_2 along the X+45 direction. All subsequent strain changes for the array on the XY surface seem to be influenced by these directions.

Once rosettes 2-13 were mounted (Figure 1) the 15-cm overcore was drilled. The depth of this overcore and of the 10- and 5-cm overcores was held to 9 cm to prevent intersection of the macrofractures parallel to the XY surface in the bottom half of the block. Strain changes after stabilization (68 hours) resulting from the 15-cm overcore at rosettes 1-10 show varying degrees of

relaxation with secondary principal axes oriented along the X±45° directions (Figure 6b). The cumulative strains at rosette 1 are shown in the lower-right corner of the XY face (Figure 6b), and the complete strain-change record for this rosette is listed in Table 2. Similar data are kept for all rosettes, but only those for rosette 1 are presented here. Cumulative strain changes for all rosettes are listed in Table 3; incremental strain changes after each overcore are listed in Table 4. Certain particularly significant results at this stage are as follows:

1) E_1 and E_2 at rosette 1 have the same sign and direction as in Figure 6a, but are smaller than the initial relaxations. The incremental strains at rosette 1 are, however, significantly larger than those at rosettes 2, 3, 6, 8, 9, and 10 that are all located closer to the free surfaces introduced by the 15-cm overcore.

2) E_1 at rosettes 1, 2, 3, 7, and 10 is oriented nearly parallel to E_2 at rosettes 4 and 5. This suggests the relaxed residual strains are reflecting domains in which the stored strains are at least partially compensated. For example, principal strains at rosette 5 are opposite in sign to those at the adjacent rosette 2.

3) Comparison of the response at gages 5 and 8, and 7 and 10 (Figure 6b) indicates that strain changes interior to the 15-cm overcore are larger than those exterior to the overcore.

Upon overcoring with the 10-cm drill bit, the strain changes stabilized at most gages within 100 hours. Resulting incremental strain changes (Figure 6c, Table 4) and cumulative ones (Figure 6e, Table 3) indicate the following:

1) Strain changes are small at all gages even for rosettes 5, 6, and 7 that are located on the annulus between the 15-cm and 10-cm overcores.
2) The principal axes of the strain changes continue to occur along the X+45° and X-45° directions, except at gages 1, 4, and 8 where the principal axes are rotated nearly 45° (Figure 6c).
3) Changes continue to occur at gages 8-10 that are exterior to the 15-cm overcore.
4) At gages 2, 3, 4, 5, 6, 7, 9 and 10 the incremental principal strains tend to be radially compressive and tangentially extensive relative to the concentric overcores.

Upon overcoring the 5-cm drill bit, the strain changes stabilized at most gages between 150 and 200 hours after overcoring but they did not stabilize at rosettes 3, 4, 5, and 7 for 25 days. Resulting strain changes (Figures 6d, f, Tables 3 and 4) are as follows:

1) Incremental and cumulative principal strain changes continue to occur within 30° of the X$\pm$45° directions, and six of the ten are within 10° (Table 3).
2) Principal strains at rosette 1 reversed in sense (Figure 6d) causing the net strains accumulated since just before the 15-cm overcore also to be reversed (Figure 6f). Total cumulative strain, which includes the relaxation produced by the initial test overcore (Figure 6a), remains an elongation parallel to the X-45° direction (Figure 6f, lower right corner of diagram).

3) Large strain changes occurred subparallel to the X+45° and X-45° directions at rosettes 2, 3, and 4 located on the annulus between the 10-cm and 5-cm overcores. The 5-cm overcore is not concentric and the strain changes are largest at rosette 2 located where the annulus is thinnest.

4) Strain changes still occurred at rosettes 5 through 10 even though these gages are located on the outer annuli.

5) None of the strain changes seem to be related to the opening of macrofractures under the gages.

6) Time for gage stabilization progressively increases with sequential overcoring.

The strain changes recorded on the YZ plane via the test overcore and at rosettes 11, 12, and 13 (Figures 1, 7, and Table 3) give some idea of the relaxations at angles to the XY plane. Upon test overcoring, E_1 (115×10^{-6}) is oriented in the YZ plane and at 49° to the XY plane. Upon overcoring of the XY surface, strain changes continue to occur at rosettes 11, 12, and 13 (Figure 7) such that along directions at > 45° to the XY plane each rosette records an initial contraction (15-cm overcore), then an expansion (10-cm overcore), and finally another contraction (5-cm overcore). Similarly, at angles < 45° to the XY plane the rock initially contracts, then expands at rosettes 11 and 13, while it contracts further at rosette 12, and finally it expands at all three rosettes for the 15-, 10-, and 5-cm overcoring, respectively (Figure 7). The magnitudes of the strain changes at rosettes 11-13 are about equal to those at rosettes 8-10, and are less than those at rosettes 1-6 (Table 3). The strain changes at rosettes 11, 12, and 13 illustrate the far reaching affect of the reorganization of the residual strains as the block is overcored.

Residual Strains: X-ray Data. The state of residual strain directly beneath rosette 1 was determined by X-ray diffractometry. After the 5-cm

overcore was drilled, the rosette stabilized, and final strain changes were read, the center core was removed from the block. A disc (5-cm in diameter and 1 cm thick) was cut from the top of the core, and the surface containing rosette 1 was lightly polished to remove the gages, leads, and epoxy. The X-ray measurements for seven of the ten directions required for the analysis (Friedman, 1967) were made form the top (XY) surface, and the corresponding diffraction data were obtained from the same layer of quartz grains that were in contact with the rosette. The second surface required for the X-ray analysis is oriented parallel to the Z axis and was cut from the remainder of the central core within 5-cm of the top disc.

The principal axes of the residual elastic strain calculated from the diffraction data are strongly grouped (Figure 8a). This, in itself, suggests the observed residual strains are reasonably homogeneous within the areas sampled. The observed state of residual strain is characterized by the greatest elongation (average of 100×10^{-6}) oriented subparallel to X, the intermediate principal axis (5×10^{-6}) subparallel to Y, and the least elongation (actually a compressive strain, -85×10^{-6}), subparallel to Z. Thus the principal axes of the residual strains as measured by X-rays are nearly coincident with X, Y, and Z, in marked contrast to the principal axes in the XY plane calculated from the strain-relief data at rosette 1, which are oriented along the X $\pm$ 45° directions throughout the history of strain release.

Fracture Anisotropy. Point loading tests on three mutually perpendicular sets of quartzite discs indicate that the induced tensile

fractures tend to form nearly parallel to the XY, YZ, and YZ planes (Figures 8b, c, and d, and Table 1). In spite of this strong fracture anisotropy the differences in corresponding average tensile strengths are small and are not statistically significant (Table 2). The strongest anisotropy is parallel to XY, the bedding plane, next that subparallel XZ, and least that subparallel to YZ.

Fabric. The orientation of fabric elements that might influence the fracture anisotropy and ultrasonic data were investigated initially. These include the apparent long axes of elongated grains, long grain boundaries, crystallographic c-axes, and defects within the grains--namely microfractures and deformation lamellae.

In the Sioux Quartzite the apparent long axes of grains with apparent long to short axial ratios >2.0 are essentially parallel to the long grain boundaries. The orientation of these long axes, as viewed in thin section, are statistically parallel to bedding (Figure 8e and f) and to the ZY plane (Figure 8g). The long axes and boundaries thus parallel two of the three directions of preferred tensile fracture (Figure 8b, c, and d).

The c-axes of the quartz grains are randomly oriented (Figure 9a). Thus no anisotropic behavior of the rock can be attributed to a preferred crystallographic orientation of the quartz grains themselves. The grains contain planar defects, however, that could influence the physical behavior of the rock. These are healed microfractures and deformation lamellae. The former are fractures within individual grains along which impurities are concentrated and across which there has been chemical rebonding. No fresh, unhealed microfractures are observed. The microfractures however,

are oriented diffusely and no statistically significant concentration of normals to microfractures occurs (Figure 9b).

Quartz deforation lamellae, known to be planar concentrations of dislocations and impurities (Carter, 1964), are abundant. These features exhibit a preferred orientation such that they tend to lie at angles <30° to the bedding plane, XY, (Figure 9c). Most of the grains containing deformation lamellae also exhibit undulatory extinction. It is not known to what extend deformation lamellae act as potential mechanical defects in grains, but it is known that undulose grains are preferentially fractured in experimentally deformed quartz sand aggregates (Ref. 16, p. 175).

Quartz deformation lamellae are useful criteria for the detection of the orientations and relative magnitudes of the principal stresses in the rock at the time the lamellae were produced (Ref. 17). The lamellae were studied with a view toward defining the corresponding paleostresses in order to evaluate possible sources for the residual strains and mechanical anisotropy. One technique for mapping the principal stresses involves plotting in stereographic,equal-area projection the normal to each set of deformation lamellae and the c-axis of the host quartz grain and connecting these points with the arc of a great circle. An arrow is placed at the end of the arc corresponding to the normal to the lamellae (Figure 9d, e, and f). It has been verified empirically that the arrows points toward σ_3, the least compressive principal stress, and away from σ_1, the greatest compressive principal stress (Ref. 17, p. 773). Lamellae-arrow diagrams for each of the three mutually perpendicular thin sections of the quartzite show that the arrows point toward the Z axis. Thus

Z corresponds to σ_3 of the paleostress field. The arrows point toward Z from all directions in the plane normal to Z so that it is not possible to uniquely locate $\sigma_1$or σ_2 other than to infer that σ_1 and σ_2 were about equal in magnitude and lie in the XY plane.

Transgranular-Intergranular Fracture. The T/I ratios along eight tensile fractures induced in three quartzite discs by point loading were measured to determine if this ratio would vary with fracture orientation and/or loading direction. T/I ratios vary from 1.0 to 2.6 with a tendency for the lower ratios to occur along fractures oriented parallel to bedding (the XY plane). This observation along with the overall smaller ratios as compared with the Charcoal Granite suggest that grain boundaries play a larger role in the fracture of the quartzite than they do for the granite.

Ultrasonic Data. The average ultrasonic velocity field for the Sioux Quartzite has orthorhombic symmetry with the minimum velocity (between 4.9 and 5.0 km/sec) parallel to Z, the intermediate velocity 20-30° clockwise from Y in the XY plane, and the axis of greatest velocity (> 5.4 km/sec) 20-30° clockwise from X (Figure 5b). The greatest and intermediate velocity axes are within 20° of the X+45° directions and, therefore, are within 20° of the principal axes of residual strain, E_1 and E_2 as determined by strain relief. The average velocity is much lower than that expected for unfractured quartz (≃ 6.05 km/sec) which suggests the rock contains abundant microfractures or openings along grain boundaries. From the velocity pattern one would predict a strong set of microfractures or other plane anisotropy parallel to XY (i.e., the bedding plane) and perhaps a secondary set

of microfractures inclined at 20-30° to the XZ plane.

The attenuation pattern is almost cubic in symmetry (Figure 5e). The pattern, in terms of signal amplitude variations, suggests a major set of microfractures or the bedding plane oriented perpendicular to the Z axis. The pattern also suggests two other sets of microfractures, oriented parallel to the YZ and XZ planes. The best signals are transmitted along those directions for which the direction cosines from X, Y, and Z are equal. These directions are equivalent to the corners of a cube whose faces are parallel to the three sets of mutually perpendicular microfractures or some other form of mechanical anisotropy.

Berea Sandstone

Description. The block of Berea Sandstone measures 29.7 cm by 29.4 cm by 21.4-cm, contains no macroscopic fractures, and exhibits thin (≈ 1.0 mm), distinct, bedding laminae parallel to the XY surface. The rock is a grey, fine-grained sandstone (median grain size about 0.2 mm), with 22 percent porosity. Its framework grains consist of quartz (70 percent), polycrystalline quartzose rock fragments (25 percent), and feldspar (5 percent). Interstitial areas contain clay and some calcite cement in a ratio of 7:1, respectively. Bedding is manifest by dimensional alignment of detrilal grains (Figure 12), concentrations of fine detritus, and of heavy minerals. The rock is indurated primarily by pressure solution and overgrowths at quartz-quartz grain contacts. These vary from points to sutured, most are trangential. The detrital quartz grains contain some deformation lamellae and healed microfractures, but very few fresh unhealed microfractures are observed in thin section.

Residual Strains: Strain-Relief Data. Upon initial test overcoring,

the rosette on the YZ surface (Figure 1) and rosette 1 stabilized after 90 hours. Initial strain changes on YZ surface were expansions of 200, 400, and 110 ($x10^{-6}$) for gages a, b, and c, respectively. At the same time rosette 1 contracted: -130, -180, and -160, at gages a, b, and c, respectively. An hour later the strains at both rosettes reversed from their initial expansions and contractions. Between 1 and 16 hours after overcoring gage c of the YZ rosette expanded dramatically to 1,100 and gage c at rosette 1 contracted to -400. In neither case were these large changes accompanied by fracturing under the gages or any form of electrical (i.e., technique) errors. Final strain changes at the YZ rosette are -10, 200, and 1,115 and those at rosette one are -80, -205, and -400, at gages a, b, and c respectively. The secondary principal strains at rosette 1 are shown in Figure 10a. There is no reason to doubt the validity of these large strains.

Rosettes 2-13 were then mounted, tested for stability, and the XY surface was overcored to a depth of 15 cm with the 15-cm diameter drill bit. Strain changes stabilized after 190 hours and those at 240 hours were used to calculate the principal strain changes (Figure 10b). Significant aspects of the strain changes are as follows:

1. Incremental principal strain axes, i.e., those resulting only from the 15-cm overcore, are all within 25° of being radial and tangential relative to the overcore, but no clear pattern of compressions or expansions along these directions is evident.
2. Strain changes outside the 15-cm overcore are smaller than those inside.
3. Strains at rosettes 6 and 7, nearest the overcore, are larger than at other rosettes, but the changes at rosettes 1 and 2

are larger than those at rosette 5 which is closer to the introduced free surface.

4. Strains at rosette 1 are expansions while for the test overcore they were contractions (Figure 10a). The cumulative strains changes at rosette one are shown in the lower right corner of Figure 11b.

Principal axes of the incremental and cumulative strain changes after the 10-cm overcore are shown in Figures 10c and e, respectively. The strain changes from which the principal axes were calculated were read 25 days after overcoring. Aspects of the results are as follows:

1. Incremental strains at rosettes 1-10 are all compressive whereas most were expansions after the 15-cm overcore (compare Figure 10 b and c).
2. Incremental strain axes at rosettes 2-7 are all within 20° of radial and tangential directions.
3. Strains at rosettes 8-10 continued to change, but, as before, the changes are smaller than those at gages 1-7.
4. Strain changes tend to be largest at those rosettes adjacent to the free surface of the 10-cm overcore.
5. Cumulative strains are compressional along radial directions and extensional along tangential directions (Figure 10e). At all but rosette 2, the principal axes are within 20° of being radial and tangential.

After the 5-cm diameter overcore most of the gages stabilized after 12 to 14 days, but they were monitored through the 24th day. Values used to calculate the incremental and cumulative principal axes (Figure 10d and f,

Tables 5 and 6) are the averages taken from the last 7-10 days of the record. In general those gages recording the largest strain changes take the longest to stabilize. Relaxation data of particular interest resulting from the 5-cm overcore are as follows:

1. Incremental strains occur at all rosettes. As a whole they are smaller in magnitude then those resulting from the 10-cm overcore (Compare Figure 10c and d). Whereas the incremental principal strains were all compressive after the 10-cm overcore they are of mixed sign after the 5-cm overcore.
2. The strain change at rosette 5 (Figure 10d) is the largest within the array even though this rosette lies on the annulus between the 15-cm and 10-cm overcores.
3. Incremental principal strain axes at rosettes 2-9 are within 20° of the radial and tangential directions as are those of the cumulative strains for rosettes 2-10 (Figure 10d and f).
4. Principal axes of the cumulative strains at rosettes 2-10 are radially compressional and tangentially extensional.
5. At rosette 1 the principal strain changes remain throughout the relaxation history subparallel to the X and Y axes of the block. Subparallel to Y the principal strain initially contracted (Figure 10a), then expanded (Figure 10b), and then contracted again (Figure 10c, d). The overall cumulative strains shown in the lower right corner of Figure 10f, indicate a compressive strain (-330×10^{-6}) subparallel to Y and a small extension (20×10^{-6}) subparallel to X.

The strain changes on the YZ plane via the test overcore and those at rosettes 11, 12, and 13 (Figure 11, Tables 5 and 6) give data on

relaxations at angles to the XY surface. Upon test overcoring E_1 (1250×10^{-6}) is oriented 70° below the +Y axis in the YZ plane; E_2 (-55×10^{-6}) correspondingly lies at 20° to the XY plane. Upon sequential overcoring of the XY surface strain changes occur continually at rosettes 11, 12, and 13 (Figure 11) such that initially expansions occur (15-cm overcore), then contractions (10-cm overcore), followed by expansions (5-cm overcore). Strain changes resulting from the 15-cm overcore are larger than those for subsequent overcoring, and are comparable in magnitude to those at rosettes 1-10 on the XY surface. Subsequent changes are in the main smaller than those on the XY surface.

There does not appear to be any consistant trend in the orientation of the cumulative principal strain changes at rosettes 11-13. Cumulative E_1 axes are oriented at >45° to the XY plane at rosettes 11 and 12, and are <45° to XY at rosette 13. The initial E_1 expansion at rosette 12 (15-cm overcore) is within 7° of being parallel to that recorded for the test overcore.

Residual Strains: X-ray Data. The residual strains were measured twice. The first set of data is from the test overcore (Figure 12a) and the second set is from the 5-cm overcore about rosette 1 (Figure 12b). In both instances the electric gages, leads, and epoxy were removed by light polishing so that 7 of the 10 measurements required by the X-ray technique were made from the same layer of grains that yielded the strain-relief data.

Similarities and differences between these two solutions (Figures 12a and b) are as follows:

1. The principal strain axes from the test overcore are more tightly grouped than are those under rosette 1 suggesting a somewhat higher degree of homogeneity for the former.
2. Magnitudes of the average principal strains are in reasonably good agreement in light of the $\pm$ 20 x 10^{-6} accuracy of the technique.
3. Their average orientations are not coincident, but they do lie in similar quadrants. The greatest elongations(X) are 35° apart, and the intermediate (O) and the least elongations (●) are each 55° apart.

Although the differences between the two sets of X-ray measurements are significant, the agreement that does exist suggests the residual strains in the block are not totally heterogeneous. The magnitudes of the residual strains still locked in the quartz grains are small compared to most of the incremental strain changes observed upon overcoring.

Fracture Anisotropy. Point loading tests on three mutually perpendicular sets of oriented discs taken from the block indicate a strong tendency for the rock to fracture nearly parallel to bedding (XY plane), and to a lesser extent, parallel to the XZ plane (Figure 12c, d, and e and Table 1). The former is accompanied by a tensile strength anisotropy (Table 1).

Fabric. As for the quartzite, fabric elements that might influence the mechanical and physical properties of the Berea Sandstone were studied in detail. The most conspicuous and influential of these is the sedimentary bedding previously described. Other elements investigated include apparent long grain axes, quartz c-axes, and intragranular defects--microfractures and quartz deformation lamellae.

The apparent long axes of the detrilal grains as seen in thin section reflect not only the orientations of the elongate grains but also the corresponding long grain boundaries and adjacent elongated interstitial areas. The bearings of these long axes for grains with apparent long to short axial ratio of ≥ 2.0 are strongly oriented parallel to bedding (Figure 12f and g). Within the bedding plane they are somewhat oriented along the X+45° direction (Figure 12h). It is significant that the tensile fractures induced by point loading normal to the XY plane are parallel to the XZ plane and appear to ignore the trend of the apparent long axis along the X+45° direction (Figure 12c and h).

Crystallographically the quartz grains are randomly oriented (not illustrated). About 44 percent of the framework quartz and feldspar grains are undeformed, 41 percent contain healed microfractures, another 7 percent exhibit fresh microfractures, 4 percent contain deformation lamellae, and 5 percent exhibit twin lamellae. The microfractures and quartz deformation lamellae are randomly oriented (Figure 13).

Transgranular-Intergranular Fracture. The tensile fractures induced by point loading propagate intergranularly almost exclusively. This holds for fractures parallel or normal to bedding. Accordingly, the T/I ratio is zero, and factors that influence the fracture anisotropy must also be intergranular.

Ultrasonic Data. The ultrasonic velocity and attenuation data for the Berea Sandstone exhibit nearly similar symmetry elements (Figure 5c and f, respectively). The major difference is that the minimum velocity < 2.70 km/sec is inclined at 20°-30° to Z whereas the minimum amplitude signal coincides with Z. Otherwise the planes of highest and lowest velocity, highest and lowest amplitude, and the XZ plane are within 20° of being parallel. The intermediate velocity is inclined 10° to Y, but the overall trend of the relative amplitudes suggests the intermediate attenuation is inclined at 30° to Y, i.e., 40° to the intermediate velocity.

The minimum velocity and relative amplitude nearly parallel to Z reflects the mechanical anisotropy of the sedimentary bedding (XY-plane). The intermediate velocity and relative amplitude, both subparallel to Y, suggest a second but weaker set of defects oriented nearly parallel to the XZ plane. The largest velocities and best signal would be along the intersection of the two sets of defects.

DISCUSSION OF RESULTS

The residual strains, fracture anisotropy, fabric, and ultrasonic velocity and attenuation in blocks of Charcoal Granite, Sioux Quartzite, and Berea Sandstone have been studied to determine (a) the cause and effect relations among these attributes, and (b) to what degree a knowledge of the residual strains, fabric, or ultrasonic data can be used to predict fracture anisotropy or other aspects of the mechanical behavior of rocks. Toward these ends the wealth of data presented in the previous section can be synthesized by focussing attention on the relaxation of residual strains, the correlation between residual strains detected by strain relief and those determined by X-ray diffractometry, factors that influence fracture anisotropy, and prediction of the fracture anisotropy.

Relaxation of Residual Strains

This topic is of considerable importance in applied rock mechanics in that residual stresses (strains) plus the applied loads constitute the in situ state of stress. Attempts to measure the in situ condition by means of strain relief will also involve relaxations of the residual strains. Hence an understanding of the latter will help us to interpret the former. In addition, sonic interrogation of the rock mass with a view toward inferring the mechanical properties of rock also involves consideration of the residual stresses (Ref. 7) so that an independent measure of the residual strains in the rock mass would be desirable.

Detailed study of the release of residual elastic strain in the blocks of Sioux Quartzite and Berea Sandstone, the similar previous work of Nichols on the block of Barre Granite (Ref. 11), and recent field study of strain relaxations in the Cedar City Quartz Diorite by Swolfs, Pratt, and Handin

(Ref. 18) all show conclusively that there is a definite pattern to the relaxations from which certain generalities can be recognized. As a result our understanding of the subject is much improved. The reader might wish to review the details of the relaxation history for the blocks of Sioux Quartzite (p. 17) and Berea Sandstone (p. 26). The generalities of the strain release are as follows:

1. Each time a new free surface is introduced into the test block or specimen the residual strains reorganize into a new state of internal equilibrium. This reorganization (partial relaxation) apparently involves transmission of stress throughout the block in that strain changes occur at all rosettes mounted on the surfaces of the block including those separated from the latest overcore by previous overcores (Figures 6 and 10).

2. Many of the principal incremental strains and nearly all of the principal cumulative strains at each rosette tend to be compressions in radial directions and expansions in tangential directions relative to the concentric overcores. In the field test of Swolfs and others (Ref. 18) the outcrop was relieved by vertical slots arranged in a rectilinear pattern. The calculated principal residual strain axes are compressions normal to the slots and expansions parallel to them, while at the corners they are oriented along diagonal directions.

3. In most instances, but significantly not in all, the principal strain changes at rosettes located closest to the introduced free surfaces are larger than those at more distant locations. Moreover, particularly for the 15-cm overcore, the strain changes at locations internal to the overcore tend to be larger than those at exterior but equidistant locations.

4. The principal incremental strain changes at a given rosette tend to vary in orientation, magnitude, and/or sign (compression or extension) from

one overcore to the next (e.g., compare Figure 10b and c). This raises serious questions as to the significance of residual strain measurements or of in situ "stress" measurements in blocks with residual strains when done with a single overcore.

5. Exceptions to the generalities expressed in (2) and (3) could simply be due to heterogeneities in material properties or in the residual strain field. On the other hand, some of these exceptions are systematic, e.g., orientation of principal strain axis along the XY radius of the block of quartzite (Figure 6) or those along the X-45° radius in the block of sandstone (Figure 10). As such, the systematic exceptions are interpreted as evidence that the "virgin" residual strain field in each block before overcoring also influences the orientations and magnitudes of the relaxed strains.

From the above generalities it is reasonable to conclude that relaxations of residual strains seem to be controlled by superpositions among (a) the "virgin" condition of residual strain, (b) the distance to the introduced free surfaces, (c) the shape of the free surfaces, and (d) the shape of the test block or specimen. It follows that the residual strain field at the time it was initially locked-in probably undergoes modification at least from natural fragmentation of the rock mass due to fracturing, removal of the specimen from the rock mass, and the act of overcoring or some other form of strain relief. It is very probable therefore, that the residual strain field in a rock mass is heterogeneous,even if initially homogeneous, in that within at least 10 to 25 centimeters of each joint surface the residual strains may have changed to reflect the introduction of a free surface in the manner of generality (2). The degree of homogeneity probably increases with increasing joint spacing. Even if the rock mass remains statistically homogeneous with

respect to the residual strains extreme caution ought to be exercised in extrapolating to the rock mass the measurements obtained from individual blocks because the acts of collecting and overcoring clearly influence the results. In spite of generalities (2) and (4) and the logical conclusions expressed above there are data that indicate good correlations exist between principal residual strains, determined from strain-relief and X-ray techniques, and the geological framework from which the specimens were taken (e.g., Hoskins and others, Refs. 19, 20; Gay, Ref. 21; De la Cruz, in Ref. 7; and Friedman, Ref. 7, among others). No ready explanation is offered for the conflict between the conclusions reached here and the empirical measurements from the field.

Further, it is not clear from the strain-relief measurements what data, if any, can be used to characterize the virgin residual strain field in each test block. Intuitively one might expect the relaxation of the block upon initial introduction of a free surface (the test overcore, Figure 1) to yield the desired data. This is perhaps supported by the strain changes along the X-Y radius in the block of Sioux Quartzite which deviate from generality (2) along directions defined at rosette 1 after the initial test overcoring (Figure 6). However, the experimental design adopted in this study is inadequate to test this view because (a) only rosette 1 was mounted during the test overcore so that we have no idea how homogeneous the initial strain changes might be; and (b) the location of the test overcore might have itself influenced the response. It would have been better to drill the test overcore into the bottom surface of the block directly opposite rosette 1 and after all the gages had been mounted. This would have at least imposed an axially symmetric free surface under rosette 1. In any case, it will be shown in the discussions to follow

that there is essentially little correlation between the residual strains measured by strain relief with those measured by X-ray diffraction or with the fracture anisotropy, fabric, or ultrasonic data.

One further point concerns the validity of borehole-gage determinations of the in situ state of stress in rock with residual strain. This point was made by Nichols (Ref. 11), and is worth repeating here. Generality (2) holds that the principal residual strain axes tend to be compressional along radial directions and extensional along tangential ones. Consider the ramification of the contractions along any radial direction on a borehole measurement (Figure 14a). The contractions upon strain relief in the center core and outer annulus relate to the relaxation of tensional strains/stresses. In a borehole measurement the device is placed in a pilot hole and then overcored. The overcore will result in a radial contraction of the annulus which will cause the borehole device to register an expansion (Figure 14b). Normally this would be interpreted as reflecting the relaxation of a compressional stress. Thus the borehole measurement is apt to be misinterpreted when employed to measure the in situ state of stress in rocks for which the residual stresses (strains) are relatively large compared to the applied loads.

Comparison of Strain-Relief and X-ray Residual Strain Data

The nature of the correlation between the data from the two techniques for measuring residual strain is important in that it helps to interpret the relaxation data and enhances understanding of the residual strain phenomena. The Charcoal Granite gives a result not observed previously (Ref. 7). No relaxations of residual strains are recorded as a result of overcoring, yet residual strains are measured in the quartz by X-ray

diffractometry (Figure 3a). Recall that the quartz makes up only about 25 percent of the rock by volume, occurs in the interstices within a load-bearing framework composed essentially of feldspar crystals, and is about 10 percent the size of the feldspars. Either the strains measured in the quartz are permanent and there are no recoverable strains in the feldspars, or upon overcoring the contractions and expansions in all crystals under the gages of the rosettes cancel, or the quartz alone contains residual elastic strain. The gages are 2 by 4 mm and the grain size varies from <0.1 to 10 mm. If the strains in the quartz are potentially recoverable then the residual stresses giving rise to these strains are in equilibrium (compensated) within very small domains, less than the size of the larger grains. The existance of residual strains in the quartz and the lack of them in the larger feldspar crystals suggests that those in the quartz may have occurred as a result of the negative volume change upon cooling from high-quartz (ρ = 2.53 g/cc) to low quartz (ρ = 2.65 g/cc). In any event, the strains in the quartz species are different from those in the other crystals that make up the bulk of the rock.

Results from the blocks of Sioux Quartzite and Berea Sandstone permit direct comparison between the strain-relief and the X-ray data. The comparison is made primarily between the cumulative and incremental strains at rosette 1 and the X-ray data taken largely from quartz grains located directly underneath rosette 1. For the Sioux Quartzite, the incremental and cumulative strain changes at rosette 1 are consistently oriented along the X $\pm$ 45° directions (Figure 6). In contrast, the principal strain axes calculated from the X-ray measurements are nearly parallel to the X, Y, and Z coordinate axes (Figure 8a). The locked-in compressive strain nearly parallel to Z (Figure 8a) is not reflected by corresponding principal extensive strains in the strain-relief data at the test overcore rosette

or at rosettes 11, 12, and 13 (Figure 7). Thus a very poor correlation exists between the two sets of data for the quartzite. It will be shown later, that the X-ray data is fully compatable with the fracture anisotropy in the rock while the strain-relief data are not.

For the Berea Sandstone, the incremental and cumulative strain changes at rosette 1 indicate a large contraction nearly parallel to the Y axis (Figure 10). This corresponds to the relaxation of a tensile stress subparallel to Y. Both X-ray determinations (Figure 12a and b) give principal axes at large angles to X, Y, and Z, and residual strain magnitudes parallel to Y are essentially zero. A small compressive strain (-30×10^{-6}) occurs parallel to Z in both solutions of X-ray data while strain changes upon strain relief of the test overcore rosette reflect a very large compressive stress oriented at 20° to the Z axis. Accordingly, as in the case of the quartzite, a very poor correlation exists between the two sets of residual strain data. Although instances of good correlation have been encountered, in general correlations tabulated for 16 or more sets of strain-relief and X-ray data are poor (Ref. 7, Table IV). Possible explanations for the poor correlations are given elsewhere (Ref. 7).

Factors That Influence Fracture Anisotropy

Charcoal Granite. Point loading tests indicate a tendency for this rock to fracture at 10° or so to the XY plane (Figures 3b, c, d, Table I). The cause(s) for this fracture anisotropy is explored in the X-ray residual strain and fabric data.

Relative to the residual strains, the orientation of tensile fractures induced by point loading can be predicted (e.g., Figure 3a, dashed line) on the assumptions that (1) the fractures will be controlled solely by the net stress field resulting from superposition of the point load on the state

of residual stress (strain), and (2) the fractures will form perpendicular to the net least compressive stress σ_3 and parallel to the net $\sigma_1\sigma_3$ plane (Ref. 6). The point load itself produces an axial compressive stress, σ_1, parallel to the direction of loading and a tensile stress uniform along all radii in the plane normal to the point load. Thus the net σ_1 will always parallel the direction of loading and the net σ_3 will lie in the plane of each disc parallel to the direction of the residual stress that is least compressive (or most tensile).

For the Charcoal Granite it is clear that the induced tensile fractures are inclined about 10° to the XY plane if the point load is applied parallel to either the X or Y axis. For both these orientations the average greatest residual elongation is nearly perpendicular to the average trend of the fractures (Figure 3). Thus upon superposing the point load on the residual stresses the net greatest principal tension (σ_3) coincides with the greatest residual elongation, and the intermediate principal stress will be X or Y as the case may be. Moreover, when the point loading is parallel to Z a nearly random pattern of tensile fractures occur, perhaps because the residual strains (stresses) in the XY plane are nearly equal.

Previously it was noted that the observed residual stresses in the quartz are reasonably homogeneous throughout the X-ray sample, but that they may be compensated within very small domains. If the latter is true they might not be expected to influence bulk properties such as fracture anisotropy. Clearly, however the observed state of residual strain is fully compatible with the fracture anisotropy. That is, the trend of the fractures including their slight angle to the XY plane can be predicted from superposition of the point loads on the observed state of residual strain.

Fabric elements that might also control the fracture anisotropy are any kind of homogeneous, pervasive feature that could serve as a defect or plane of mechanical discontinuity. The measure of an element's influence on the fracture anisotropy has to be judged on whether or not its orientation pattern consistently occurs parallel to the trend of the induced fractures.

Consider first the traces of long grain boundaries as observed in three mutually perpendicular thin sections. These are not only potential planar flows, but they serve to define the orientation of the feldspar crystals which form most of the long boundaries and the load bearing framework of the rock. The trend of the tensile fractures when point loading is parallel to Y (Figure 3b) is parallel to the long boundaries in the XZ plane (Figure 3f). Similarly the fracture trend for loading parallel to X (Figure 3c) is accompanied by a strong orientation of long axes (Figure 3g). However, the tensile fractures are statistically random when loading parallel Z, (Figure 3d, Table 1). The corresponding long boundaries are scattered although some are clustered at small angles to the YZ plane. Thus for two of the three loading directions the fractures do follow the traces of the long grain boundaries, and when the grain boundaries are scattered so are the induced tensile fractures. Accordingly, the long grain boundaries cannot be excluded from exercising control on the fracture anisotropy even though the high transgranular-to intergranular ratios suggest that fabric elements internal to the grains rather than grain boundaries are more apt to control fracture orientation in this rock.

Internal to the grains, the microfractures are the only type of planar defect that exhibit preferred orientation (Figure 4b, c, and d). They are strongly oriented parallel to the XY plane and somewhat less so parallel XZ and YZ planes. Accordingly the microfractures also could contribute to

the strong fracture anisotropy parallel to XY.

In summary, the fracture anisotropy in the Charcoal Granite could be caused by one or more of three factors: the residual strains, the oriented framework of feldspar crystals as measured through long grain boundaries, or by intragranular microfractures.

Sioux Quartzite. Tensile fractures in this rock form preferrentially parallel to the original bedding XY and nearly parallel to the XZ and YZ planes (Figures 8b, c, and d). Again possible causitive factors are sought in the residual strains, and the rock fabric.

The residual strains from strain-relief data are eliminated immediately in that the principal axes (rosette 1) are consistently oriented along X $\pm$ 45° directions (Figure 6) while the fractures from parallel to the XY, XZ, and XZ planes.

The residual strains measured by X-ray diffractometry are another matter (Figure 8a). Point loading parallel to Z will result in the net σ_3 oriented parallel to the X axis such that the induced fractures would parallel the YZ plane (Figure 8a, dashed line). Point loading parallel to X would promote tensile fractures parallel to the bedding (XY plane) because of the strong influence of this plane of mechanical discontinuity. In addition, however, fractures would also parallel the XZ plane (Figure 8a, solid line), because for loading parallel to X, the net σ_3 would lie parallel to Y. Similarly point loading parallel to Y should result in fractures parallel to the YZ plane because then the net σ_3 would lie parallel to X. These predictions are correct for each loading direction (Figure 8b, c, and d). Thus, again, the observed state of residual strain as determined from X-rays is fully in agreement with the fracture anisotropy and could be the controlling factor if it acts as a pervasive prestress.

With regard to the fabric, consider first the apparent long grain axes (equivalent to long grain boundaries). These may be particularly important in controlling the fracture anisotropy in as much as the tensile fractures propagate along grain boundaries 50 to 30 percent of their length, i.e. T/I ratios vary from 1 to 2.6. The long grain axes define the bedding plane XY (Figure 8e and f) and coincide with the trace of the YZ plane (Figure 8g). Indeed tensile fractures do occur along these planes, but the fractures also occur along the XZ plane when loading is parallel to X and along the YZ plane when loading is parallel to Y (Figure 8c and d). Corresponding long axes to control these tensile fractures do not occur (Figure 8e and f). Thus the long axes and associated grain boundaries do not by themselves control the orientation of the tensile fractures.

The orientation patterns of intragranular fabric elements also would seem to eliminate them as exerting controls on the fracture anisotropy. Quartz c-axes, a partial measure of any crystallographic orientation of the grains in the rock, are randomly oriented (Figure 9a). Also nearly random are healed microfractures within the quartz (Figure 9b). Only the quartz deformation lamellae are non-random, these planar elements tend to lie at about 30-40° to the XY plane (Figure 9c), but this orientation pattern does not coincide with the orthogonal fracture anisotropy. The quartzite does not contain any other fabric elements that possibly might influence its fracture anisotropy.

In summary, the fracture anisotropy in the Sioux Quartzite is fully consistent only with the observed state of residual strain as measured by X-ray diffractometry. Long grain axes (boundaries) define bedding and one other plane of preferred fracture, but they can not account for the third direction of fracture. Intragranular fabric elements are either randomly or inappropriately oriented to influence the fracture anisotropy.

Berea Sandstone. Fracture anisotropy in this rock is strongly controlled by sedimentary bedding (Figure 12c and d). In addition there is a tendency for the rock to fracture parallel to the XZ plane when point loaded parallel to Z (Figure 12e). Two sets of 30 discs each were point loaded parallel to Z to double check this fracture trend. The data are essentially identical, and only data from the first set are reported (Figure 12d, Table 1). Fracture controlled by bedding is commonplace, and further explanation is not needed. The tendency to fracture parallel to XZ when loaded normal to bedding, i.e., anisotropy of bedding is neutralized, does need to be accounted for.

The incremental and cumulative strain changes from strain-relief data at rosette 1 indicate large contractions subparallel to the Y axis. This relates to the relaxation of a locked-in tensile strain or stress. It follows that the net σ_3 upon point loading parallel to Z would nearly coincide with Y. Hence tensile fractures perpendicular to Y would be consistent with the residual strains as measured by strain relief.

The residual strains determined by X-ray diffractometry, however, are not compatible with the fracture anisotropy. The predicted trends for the induced tensile fractures (Figure 12a, b, dashed lines) do not coincide with the XZ plane.

With regard to the fabric, the apparent long grain axes adequately define bedding (Figures 12f and g). Within the bedding plane they trend nearly parallel to the anticipated fracture trends from the X-ray residual strain data (compare Figures 12a, b, and h), but they do not coincide statistically with XZ plane. Accordingly their influence on this aspect of the fracture anisotropy is doubtful.

Internal to the grains, the c-axes are random (not illustrated) as

are the healed microfractures and quartz deformation lamellae (Figure 13). Fresh, unhealed microfractures are rare, and other fabric elements of possible mechanical significance do not occur.

In summary, the fracture anisotropy parallel to bedding in the sandstone was expected. That parallel to the XZ plane can be explained only by the residual strains as detected by strain relief at rosette 1. Clearly, the results for this rock stand in marked contrast to those for the granite and quartzite, for which the strain-relief data did not agree while the X-ray residual strain data and some fabric data did agree with the fracture anisotropy.

Prediction Of The Fracture Anisotropy.

In applied rock mechanics projects such as rapid underground excavation a reliable and practical method is needed for detecting fractures or for predicting mechanical anisotropy of the rock mass. Above it is shown that a knowledge of residual strains and of certain aspects of the fabric could have been used to predict the fracture anisotropy to a varying degree. The use of residual strain data is fraught with difficulties, and fabric work beyond the mapping of macroscopic planes of mechanical discontinuity is time consuming. Both require the collection and laboratory analysis of specimens. As a result neither method is attractive from a pragmetic viewpoint even if the results were totally reliable. Sonic interrogation of the rock mass, on the other hand, is attractive, provided the sonic data can be used to predict the mechanical properties. Hence it is important to evaluate the degree to which the ultrasonic velocity and attenuation data correlate with the information on residual strain and fabric, and, in turn, can be used to predict the fracture anisotropy in the three rocks.

Velocity data (Figure 5a) for the Charcoal Granite suggest microfractures are oriented at small angles to the XY plane. Moreover, the low mean velocity suggests the microfractures are abundant. These predictions or interpretations are accurate (Figure 4b, c, and d), although other intragranular planar defects such as cleavages, and exsolution lamellae may also influence the velocities. The velocity field also correlates with the residual strains determined by X-rays (Figure 3a). The minimum velocity, parallel to Z, is within 30° of the average greatest principal elongation. In that velocity increases with increasing normal stress (primarily due to crack closing), one should expect the maximum and minimum velocities to coincide with the least and greatest elongations, respectively, provided the residual strains (stresses) act like stresses across the boundaries of rocks. Further, the velocities parallel to the XY plane are nearly equal as are the residual strains parallel to X and Y (Figure 3a). Thus the velocity data are in good agreement with the residual strains and the intragranular defects.

The attenuation (relative amplitude) field for the granite also indicates microfractures are oriented nearly perpendicular to Z (Figure 5d). In addition the good signal in the Y direction and the poor one parallel to X suggests another somewhat weaker, set of planar mechanical discontinuities parallel to the YZ plane. There is a small concentration of microfractures parallel to YZ (Figure 4b and d) and there is a concentration of tensile fractures developed parallel to YZ when the discs are loaded parallel to Z, i.e., when the strong anisotropy parallel to XY is neutralized (Figure 3d).

Thus for the granite the ultrasonic velocity and attenuation data correlate exactly with the residual strain and fabric data, and as a consequence can be used to accurately predict the major and minor fracture anisotropies.

For the Sioux Quartzite, the velocities define the bedding plane XY and possibly a secondary plane of mechanical anisotropy inclined 20-30° to the XZ plane. The comparatively low average velocities suggest that the rock contains abundant microfractures (Figure 5b). The attenuation data clearly indicate that the XY, YZ, and XZ are potential planes of mechanical discontinuity (Figure 5e). These interpretations are correct in the sense that they accurately forecast the three mutually perpendicular planes of fracture anisotropy (Figure 8b, c, and d). However, the inference that the ultrasonic data are controlled solely by microfractures is inconsistent with the thin section observations which show essentially no fresh microfractures, only randomly oriented healed microfractures, and a preferred orientation of quartz deformation lamellae within 30° of the bedding (XY) plane (Figure 9b and c).

Although the X-ray residual strain data is compatible with the fracture anisotropy it does not agree totally with the ultrasonic data. The symmetry planes of the ultrasonic data, particularly the attenuations, are parallel to those of the observed residual strains (compare Figures 5b, e, and 8a); however the average principal least elongation (a compressive strain) coincides with the least velocity and the greatest elongation makes a small angle with the largest compression. These are exactly opposite to the correlations found in the Charcoal Granite and Barre Granite (Ref. 7).

In summary, the ultrasonic data for the Sioux Quartzite do accurately distinguish the bedding and the two other planes of fracture anisotropy. On the other hand, the velocities and relative amplitudes do not correspond to the residual strain data or to any of the fabric elements studied. This is puzzling because the acoustic properties and the fracture anisotropy must have a cause within the rock. It is possible that very small openings (i.e., flaws) exist along grain boundaries, and influence the acoustic data and fracture anisotropy. This speculation is supported by the low T/I ratios which suggest

weakened grain boundaries.

For the Berea Sandstone, the ultrasonic data again accurately define the bedding plane which is the main plane of mechanical anisotropy in the rock (Figure 5c, f). Likewise the velocity and the attenuation data suggest the existance of the secondary fracture anisotropy parallel to the XZ plane. As for the quartzite the microfractures in the sandstone are randomly oriented and the other fabric elements investigated do not seem to be oriented such as to influence the ultrasonic data. Similarly the residual strain measured by both strain-relief and X-ray are not compatible with the ultrasonic data.

In all three rocks, therefore, the ultrasonic data accurately define all planes of preferential fracture, with the attenuation data reflecting some that are insensitive to velocity. These predictions are based on the interpretation that microfractures or some other partially open discontinuities influence the velocities and relative amplitudes and cause the fracture anisotropy. Thin section observations support this reasoning for the granite, but the study failed to detect a cause in the fabric for all the fracture trends in the quartzite and sandstone. Accordingly in massive rocks, such as the granite, a good correlation between ultrasonic data, fabric, and residual strains (via X-rays) can be expected, and any one of the three types of analyses can be used to predict fracture anisotropy. In rocks with strong planar anisotropy the planar anisotropy will tend to dominate the ultrasonic data and possibly mask correlations between these data and the residual strains.

CONCLUSIONS

Major conclusions from study of ultrasonic velocity and attenuation, residual strain, fabric, and fracture anisotropy in blocks of Charcoal

Granite, Sioux Quartzite, and Berea Sandstone are as follows:

1. The ultrasonic data accurately define all planes of preferential tensile fracture in all three rocks.

2. In massive rocks such as the granite, there are good geometric and probably genetic correlations between the ultrasonic data, intragranular planar defects such as microfractures, grain boundaries, the residual strains determined by X-ray diffractometry, and the observed fracture anisotropy.

3. For the quartzite and sandstone, rocks with strong planar anisotropy (i.e., bedding), the ultrasonic velocities and relative amplitudes can not be explained by the orientations of microfractures determined from thin section studies. The acoustical properties may be controlled by minute flaws along grain boundaries in these rocks. The overriding influence of bedding also probably interferes with the correlation between the ultrasonic and X-ray residual strain data such that only partial correlations exist, at best.

4. Fracture anisotropy in the quartzite not controlled by bedding is fully consistent with the residual strains measured by X-ray diffraction and is only partially consistent with the orientation of elongated grains.

5. Fractures in the Berea Sandstone not controlled by bedding appear to be compatible with residual strains detected by the strain-relief method.

6. Relaxation of residual strain seems to be controlled by superposition among the condition of residual strain in the test specimen before overcoring, the distance to the introduced free surface, the shape of the free surface, and the shape and size of the test specimen. The principal axes of the strain changes generally are compressional normal to the free surface and extensional parallel to it. Further, strain changes often vary in orientation, magnitude, and/or sign (compression or extension) from one concentric overcore to the next. These facts raise serious questions

as to the significance of residual strain measurements or of in situ "stress" measurements in rocks with residual strain. They also mask possible correlations between residual strains measured by strain relief and those detected by X-ray diffractometry.

7. Borehole-gage techniques to determine the state of in situ strain (stress) in rocks with relatively large components of residual strain may be misinterpreted.

REFERENCES CITED

1. Bur, T. R., Thill, R. E., and Hjelmstad, K. E., 1969, An ultrasonic method for determining the elastic symmetry of materials: U.S. Bureau of Mines, R. I. 7333, 23 p.

2. Bur, T. R., Hjelmstad, K. E., and Thill, R. E., 1969, An ultrasonic method for determining the attenuation symmetry of materials: U.S. Bureau of Mines, R. I. 7335, 8 p.

3. Willard, R. J., and McWilliams, J. R., 1969, Microstructural techniques in the study of physical properties of rock: Intern. Jour. Rock Mech. Min. Sci., v. 6, p. 1-12.

4. Friedman, M., 1967, Measurement of the state of residual elastic strain in rocks by X-ray diffractometry: Norelco Reporter, v. 14, no. 1, p. 7-9.

5. Friedman, M., 1972, X-ray analysis of residual elastic strains in quartzose rocks: p. 573-595 in Proc. Tenth Sympsoium on Rock Mechanics, Austin, Texas, May 1968, K. E. Gray, ed., Soc. Min. Eng., AIME, New York.

6. Friedman, M., and Logan, J. M., 1970, The influence of residual elastic strain on the orientation of experimental fractures in three quartzose sandstones: Jour. Geophysical Research, v. 75, p. 387-405.

7. Friedman, M., 1972, Residual elastic strains in rocks: Tectonophysics, v. 15, p. 297-330.

8. Hall, C. J., and Hoskins, J. R., 1972, A comparative study of selected rock stress and property measurement instruments: Tech. Rept. No. 2, ARPA Order No. 1579, Amend. 2, Program Code No. IFIO, Bureau of Mines Contract No., H0210030.

9. McClintock, F. A. and Argon, A. S., 1966, Mechanical behavior of materials: Reading, Massachusetts. Addison-Wesley Pub. Co., 770 p.

10. Voight, Barry, 1966. Restspannugen im Gestein: Proceedings of the First Congress of the International Society of Rock Mechanics, 2:45-50.

11. Nichols, T. C. Jr., 1971, Deformations associated with relaxations of residual stresses in the Barre Granite of Vermont: Thesis, Texas A&M Univ., College Station, Texas, 92 p.

12. McWilliams, J. R., 1966, The role of microstructure in the physical properties of rock: Testing Techniques for Rock Mechanics, STP 402, p. 175-189, Amer. Soc. for Testing and Materials, Philadelphia.

13. Murray, W. M., and Stein, P. K., 1962, Strain gage techniques: Mass. Inst. Tech., Cambridge, 687 p.

14. Willard, R. J., and McWilliams, J. R., 1969, Effect of loading rate on transgranular--intergranular fracture in Charcoal Gray Granite: Int. J. Rock Mech. Min. Sci., v. 6, p. 415-421.

15. Nur, Amos, and Simmons, G., 1969, Stress-induced velocity anisotropy in rock: An experimental study: Jour. Geophys. Res., v. 74, p. 6667-6674.

16. Borg, I., Friedman, M., Handin, J., and Higgs, D. V., 1960, Experimental deformation of St. Peter Sand - A study of cataclastic flow: in Rock Deformation, D. Griggs and J. Handin, eds., Geol. Soc. Amer. Mem., 79, p. 133-191.

17. Carter, N. L., and Friedman, M., 1965, Dynamic analysis of deformed quartz and calcite from the Dry Creek Ridge Anticline, Montana: Amer. J. Sci., v. 263, p. 747-785.

18. Swolfs, H. S., Pratt, H. R., and Handin, J., 1973, Applied and residual strain measurements in quartz diorite, Cedar City, Utah: Trans. Am. Geophy. Union, v. 54, p. 458.

19. Hoskins, E. R., and Daniells, P. A., 1970, Measurements of residual strain in rocks, Trans. Amer. Geophy. Union, v. 51, p. 826-827.

20. Hoskins, E. R., and Bahadur, S., 1971, Measurements of residual strain in the Black Hills: Trans. Amer. Geophy. Union, v. 52, p. 922.

21. Gay, N. C., 1972, Virgin rock stresses at Doornfontein Gold Mine, Carletonville, South Africa: Jour. Geol., v. 80, p. 61-80.

Table 1

Results of Point Loading Tests

Point Load Parallel to:	No. of discs	Total No. of Induced Tensile Fractures	Mean Breaking[1] strength (bars)	St. Dev. of Breaking Strengths (bars)	Preferred Orientation of Induced Tensile Fractures
Charcoal Granite					
X	28	58	295	36	yes[2] (|| to XY plane) Chi Sq. = 51
Y	25	51	275	34	yes (|| to XY plane) Chi Sq. = 36
Z	27	66	310	34	no (random) Chi Sq. = 12
Sioux Quartzite					
X	30	66	455	47	yes (|| to XY and XZ) Chi Sq. = 105
Y	30	66	480	45	yes (|| to XY and XZ) Chi Sq. = 69
Z	30	80	500	28	yes[3](sub|| to YZ) Chi Sq. = 18
Berea Sandstone					
X	30	40	53	7.6	yes (|| to XY plane) Chi Sq. = 200
Y	30	36	54	7.0	yes (|| to XY plane) Chi Sq. = 175
Z	30	66	79(82)[4]	8.3(9.4)	yes (|| to XZ plane) Chi Sq. = 69

[1] Calculated using Reichmuth's formula (see McWilliams, Ref. 13).

[2] Based upon Chi-square "goodness of fit" test of the azimuths of induced tensile fractures as compared to a uniform distribution of azimuths, (e.g., see Figure 3b, c, d).

[3] Fracture trace diagram (Figure 8b) shows considerable scatter, but a significant grouping 20° to XY plane. Overall Chi-sq value does not indicate this grouping is significant.

[4] A second set of 30 discs were tested to check on reproducibility of tendency for fractures to form parallel to XZ plane.

TABLE 2

Residual Strain Changes, Sioux Quartzite,
Rosette No. 1

Cumulative Time (hrs)	Measured Strain Changes[1]			Calculated Principal Strains[2]		
	Gage a	Gage b	Gage c	E_1	E_2	θ^3 (degrees)
After initial test overcore						
.16	48[4]	-103[4]	29[4]	180	-103	-47
150	23	-111	16	150	-111	-46
After 15 cm diameter overcore						
1.5	62[5]	21[5]	51[5]	92	21	-49
8.3	30	20	34	44	20	-50
18.8	29	13	26	42	13	-48
22.3	34	9	31	56	9	-47
24.3	41	9	33	65	9	-50
29.3	41	9	32	64	9	-50
41.3	30	0	27	57	0	-47
46.3	43	0	33	76	0	-49
63.8	31	-9	28	68	-9	-46
68.3	41	-10	31	82	-10	-48
Cumulative[6]	64	-121	47	232	-121	-46
After 10 cm diameter overcore						
95.5	36[7]	21[7]	26[7]	42	20	-58
102.5	1	21	12	22	-9	35
115.5	2	17	11	18	-5	33
155.3	-6	9	4	10	-12	32
161.3	6	11	12	13	5	28
163.3	6	12	13	14	5	27
179.3	-6	7	6	9	-9	25
185.3	-3	10	10	11	2	23
202.3	-4	7	17	17	-4	1
Cumulative	60	-114	64	238	-114	-45
After 5 cm diameter overcore						
234.3	32[8]	-12[8]	-27[8]	35	-30	-77
239.8	-8	-7	-45	0	-53	22
250.8	-25	0	-55	3	-82	35
255.8	-26	0	-54	2	-82	35
321.3	-16	-22	-60	-11	-65	18
327.3	-16	-16	-53	-8	-61	23
369.3	-49	12	-59	12	-120	43
394.3	-64	17	-54	17	-135	43
417.8	-49	44	-33	44	-126	42

Continued

TABLE 2
(Continued)

489.8	-34	40	-37	40	-111	44
522.8	-26	32	-42	32	-101	42
546.8	-44	20	-61	20	-126	42
570.8	-60	32	-57	32	-149	45
594.8	-58	44	-46	44	-148	32
666.8	-58	40	-41	40	-139	42
Cumulative	2	-74	23	100	-74	-49

1. All strains are $x10^{-6}$; expansions are counted positive; contractions are negative. Gages a, b, and c refer to the individual gages within the 45°-rosette (Figure 1). Strains listed are the changes from the initial readings (see footnotes 4, 5, 7, and 8).

2. Secondary principal strains (also $x10^{-6}$) are calculated from standard strain gages equations (see Murray and Stein, Ref. 13).

3. θ defines the angle between the direction of gage a and E_1 (see Figure 1, note sign convention). It is also calculated from equations given by Murray and Stein (Ref. 13).

4. Strain changes from initial zero state.

5. Strain changes relative to values after 150 hours, initial test overcore.

6. Cumulative changes after initial test overcore and 68.3 hours after 15 cm diameter overcore (e.g. Gage a = 23 + 41 = 64).

7. Strain changes relative to values recorded after 68.3 hours after 15 cm diameter overcore.

8. Strain changes relative to values recorded after 10 cm diameter overcore.

TABLE 3

Cumulative Residual Strain Changes[1]

Sioux Quartzite

ette No.	Overcore (cm)	Measured Strain Changes			Calculated Principal Strains		
		Gage a	Gage b	Gage c	E_1	E_2	θ (degrees)
#1	15	41	-10	31	80	-10	-48
	10	37	-3	48	90	-5	-48
	5	-21	37	7	40	-55	36
#2	15	12	-28	10	50	-30	-46
	10	21	13	4	20	5	2
	5	-52	219	141	245	-155	40
#3	15	2	4	3	5	0	36
	10	-13	-37	-16	10	-35	-47
	5	30	-37	32	100	-35	-45
#4	15	-2	46	25	50	-25	34
	10	-11	50	30	55	-35	32
	5	-62	176	140	210	-130	27
#5	15	0	65	-4	65	-70	44
	10	5	79	-8	80	-80	43
	5	14	63	24	65	-25	42
#6	15	-6	-24	-22	0	-25	-64
	10	-1	-26	4	30	-25	-48
	5	9	9	31	35	5	-68
7	15	73	31	40	85	25	-61
	10	52	24	33	65	20	-57
	5	21	8	5	20	5	-74
8	15	-32	-18	5	5	-35	-83
	10	-52	-27	6	5	-50	-86
	5	-12	-29	-15	0	-30	-48
9	15	-8	-19	-14	0	-20	-55
	10	-1	-16	-10	5	-15	-57
	5	-6	11	10	15	-10	24
0	15	-6	-13	-5	0	-15	-47
	10	1	-11	-9	5	-15	-63
	5	11	-11	-1	20	-10	-55
1	15	-3	-8	-12	-5	-10	-87
	10	6	-15	-16	10	-20	-69
	5	4	-2	-9	4	-10	2

ontinued

TABLE 3

(Continued)

12	15 10 5	-9 5 35	-16 -16 27	-12 -21 -6	-5 7 40	-15 -25 -10	-53 -74 16
13	15 10 5	-15 -14 -5	-4 3 20	-9 -12 1	-5 5 20	-20 -30 -25	34 43 41

1. Cumulative strains at all gages represent net changes after each gage had stabilized after each overcore relative to a starting point established after the test overcore (Figure 1) and before the 15 cm overcore.

TABLE 4

Incremental Residual Strain Changes[1]

Sioux Quartzite

osette No.	Overcore	Measured Strain Changes			Calculated Principal Strains		
	(cm)	Gage a	Gage b	Gage c	E_1	E_2	θ(degrees)
#1	15	41	-10	31	80	-10	-48
	10	-4	7	17	15	-5	89
	5	-58	40	-41	40	-140	48
#2	15	12	-28	10	50	-30	-46
	10	9	41	-6	40	-40	40
	5	73	206	137	210	0	54
#3	15	2	4	3	5	0	36
	10	-15	-41	-19	5	-40	-43
	5	43	0	48	90	0	-47
#4	15	-2	46	25	50	-25	34
	10	-9	4	5	5	-10	70
	5	-51	126	110	155	-95	65
#5	15	0	65	-4	65	-70	44
	10	5	14	-4	15	-15	36
	5	9	-16	32	60	-20	-54
#6	15	-6	-24	-22	0	-25	-64
	10	5	-2	26	35	-5	-60
	5	10	35	27	35	0	59
#7	15	73	31	40	85	25	-61
	10	-21	-7	-7	-5	-25	67
	5	-31	-16	-26	15	-40	50
#8	15	-32	-18	5	5	-35	-83
	10	-20	-9	1	0	-20	89
	5	40	-2	-21	40	-25	-10
#9	15	-8	-19	-14	0	-20	-55
	10	7	3	4	5	0	-30
	5	-5	27	20	30	-15	61
#10	15	-6	-13	-5	0	-15	-47
	10	7	2	-4	5	-5	3
	5	10	0	8	20	0	-42
#11	15	-3	-8	-12	-5	-10	-87
	10	9	-7	-4	15	-10	-28
	5	-2	13	7	15	-10	57
#12	15	-9	-16	-12	-5	-15	-53
	10	14	0	-9	15	-10	-6
	5	30	43	15	45	0	35

Continued

TABLE 4

(Continued)

#13	15 10 5	-15 1 9	-4 7 17	-9 -3 13	-5 5 15	-20 -10 5	34 38 54

1. Strains at each gage represent the incremental changes after each overcore relative to a starting point established after the test overcore (Figure 1) and before each successive overcore.

TABLE 5

Cumulative Residual Strain Changes[1]

Berea Sandstone

osette No.	Overcore (cm)	Measured Strain Changes			Calculated Principal Strains		
		Gage a	Gage b	Gage c	E_1	E_2	θ (degrees)
#1	15	129	91	97	140	85	-27
	10	-6	4	-11	5	-20	40
	5	-19	-37	-48	-20	-50	-7
#2	15	109	139	99	140	70	41
	10	-19	-44	-79	-20	-80	5
	5	-12	8	-52	15	-75	32
#3	15	65	94	103	105	65	77
	10	-90	-120	-36	0	-125	-58
	5	-109	-151	-9	45	-165	-60
#4	15	95	94	62	100	55	22
	10	-164	-72	-44	-35	-170	76
	5	-208	-55	25	30	-215	82
#5	15	108	112	33	125	15	24
	10	-28	10	-125	25	-175	31
	5	-14	17	-106	30	-150	30
#6	15	286	290	221	300	205	24
	10	-29	-40	-32	-20	-40	-41
	5	-24	-17	-23	-15	-30	47
#7	15	-31	-70	116	175	-90	-62
	10	-201	-151	120	155	-235	-73
	5	-182	-174	98	150	-235	-69
#8	15	7	86	13	85	-65	46
	10	-59	2	-76	5	-140	42
ntinued	5	-61	-25	-96	-20	-135	36

TABLE 5

(Continued)

#9	15	58	51	-6	65	-15	19
	10	-32	-4	-27	-5	-55	48
	5	-35	2	-48	0	-85	41
#10	15	-24	29	30	40	-35	68
	10	-50	-17	12	10	-50	88
	5	-59	-18	3	5	-60	81
#11	15	162	250	169	250	80	46
	10	36	128	57	130	-35	49
	5	44	157	105	160	-15	55
#12	15	46	77	71	80	35	62
	10	-4	-2	-1	-0	-5	81
	5	14	16	16	15	15	68
#13	15	126	61	83	155	55	-32
	10	12	40	0	40	-30	40
	5	48	21	14	50	10	-15

1. Cumulative strains at all gages represent net changes after each gage had stabilized after each overcore relative to a starting point established after the test overcore (Figure 1) and before the 15 cm overcore.

TABLE 6

Incremental Residual Strain Changes[1]

Berea Sandstone

osette No.	Overcore	Measured Strain Changes			Calculated Principal Strains		
	(cm)	Gage a	Gage b	Gage c	E_1	E_2	θ(degrees)
#1	15	129	91	97	140	85	-27
	10	-135	-87	-108	-85	-160	56
	5	-13	-41	-37	-5	-45	-27
#2	15	109	139	99	140	70	41
	10	-128	-183	-178	-95	-210	32
	5	7	52	27	55	-20	53
#3	15	65	94	103	105	65	77
	10	-155	-214	-139	-80	-210	-48
	5	-19	-31	27	45	-40	-62
#4	15	95	94	62	100	55	22
	10	-259	-166	-106	-105	-260	84
	5	-44	17	69	70	-45	88
#5	15	108	112	33	125	15	24
	10	-136	-102	-158	-100	-195	38
	5	14	7	19	25	5	-52
#6	15	286	290	221	300	205	24
	10	-315	-330	-253	-230	-340	-62
	5	5	23	9	25	-10	49
#7	15	-31	-70	116	175	-90	-62
	10	-170	-81	4	5	-170	89
	5	19	-23	-22	30	-30	-23
#8	15	7	86	13	85	-65	46
	10	-66	-84	-89	-65	-90	-15
	5	-2	-27	-20	5	-30	-30
#9	15	58	51	-6	65	-15	19
	10	-90	-55	-21	-20	-90	90
	5	-3	6	-21	10	-30	32
#10	15	-24	29	30	40	-35	68
	10	-26	-46	-18	0	-45	-50
	5	-9	-1	-9	0	-15	47
ued							

TABLE 6

(Continued)

#11	15	162	250	169	250	80	46
	10	-126	-122	-112	-110	-125	-79
	5	8	29	48	50	10	89
#12	15	46	77	71	80	35	62
	10	-50	-79	-72	-40	-80	-29
	5	18	18	17	-20	15	23
#13	15	126	61	83	155	55	-32
	10	-114	-21	-83	-20	-180	51
	5	36	-19	14	70	-20	-38

1. Strains at each gage represent the incremental changes after each overcore relative to a starting point established after the test overcore (Figure 1) and before each successive overcore.

TABLE 6

(Continued)

#11	15 10 5	162 -126 8	250 -122 29	169 -112 48	250 -110 50	80 -125 10	46 -79 89
#12	15 10 5	46 -50 18	77 -79 18	71 -72 17	80 -40 -20	35 -80 15	62 -29 23
#13	15 10 5	126 -114 36	61 -21 -19	83 -83 14	155 -20 70	55 -180 -20	-32 51 -38

1. Strains at each gage represent the incremental changes after each overcore relative to a starting point established after the test overcore (Figure 1) and before each successive overcore.

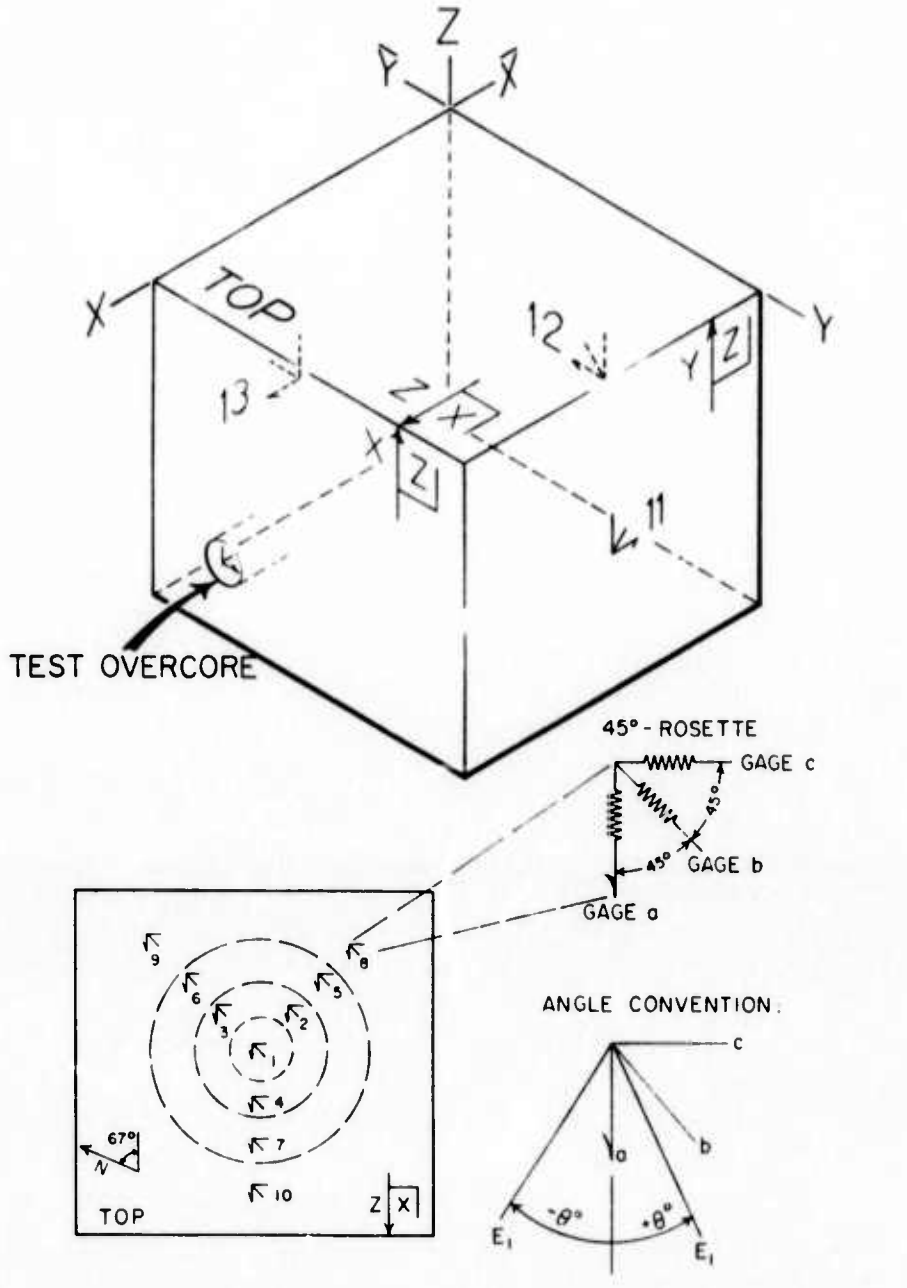

Figure 1. Orientation schemes, rosette locations, and numbers, individual gage orientation and θ angle conventions utilized in the study.

Figure 2. Block of Sioux Quartzite to be studied by strain relief procedures.

(a) The block (26.5 cm x 28.7 cm x 23 cm) is pictured with an array of ten 45°-rosette strain gages mounted on its top surface. Gages are connected through a switching unit to a strain indicator. One gage is also mounted at the center of each of the three vertical faces of the block not shown.

(b) Detail of the top surface of the block of Sioux Quartzite shows array of ten 45°-rosette strain gages and the tracings of the locations of the 15-cm, 10-cm, and 5-cm diameter overcores. All wires are disconnected during each overcore and then reconnected for measurement of strain changes.

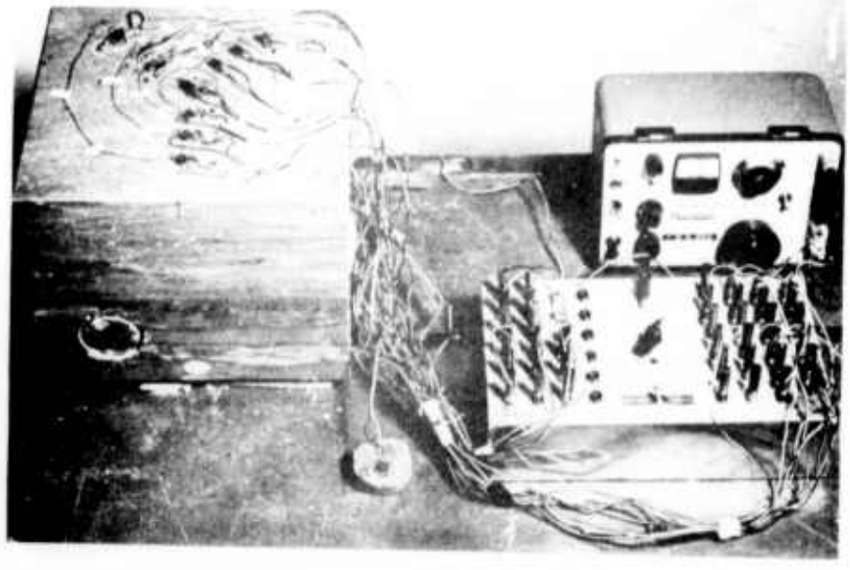

a

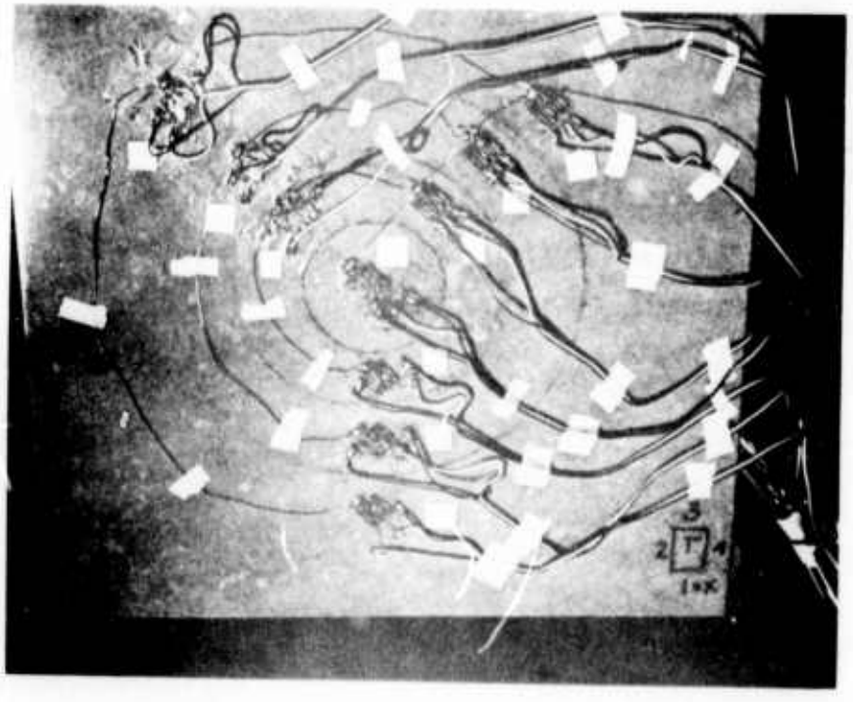

b

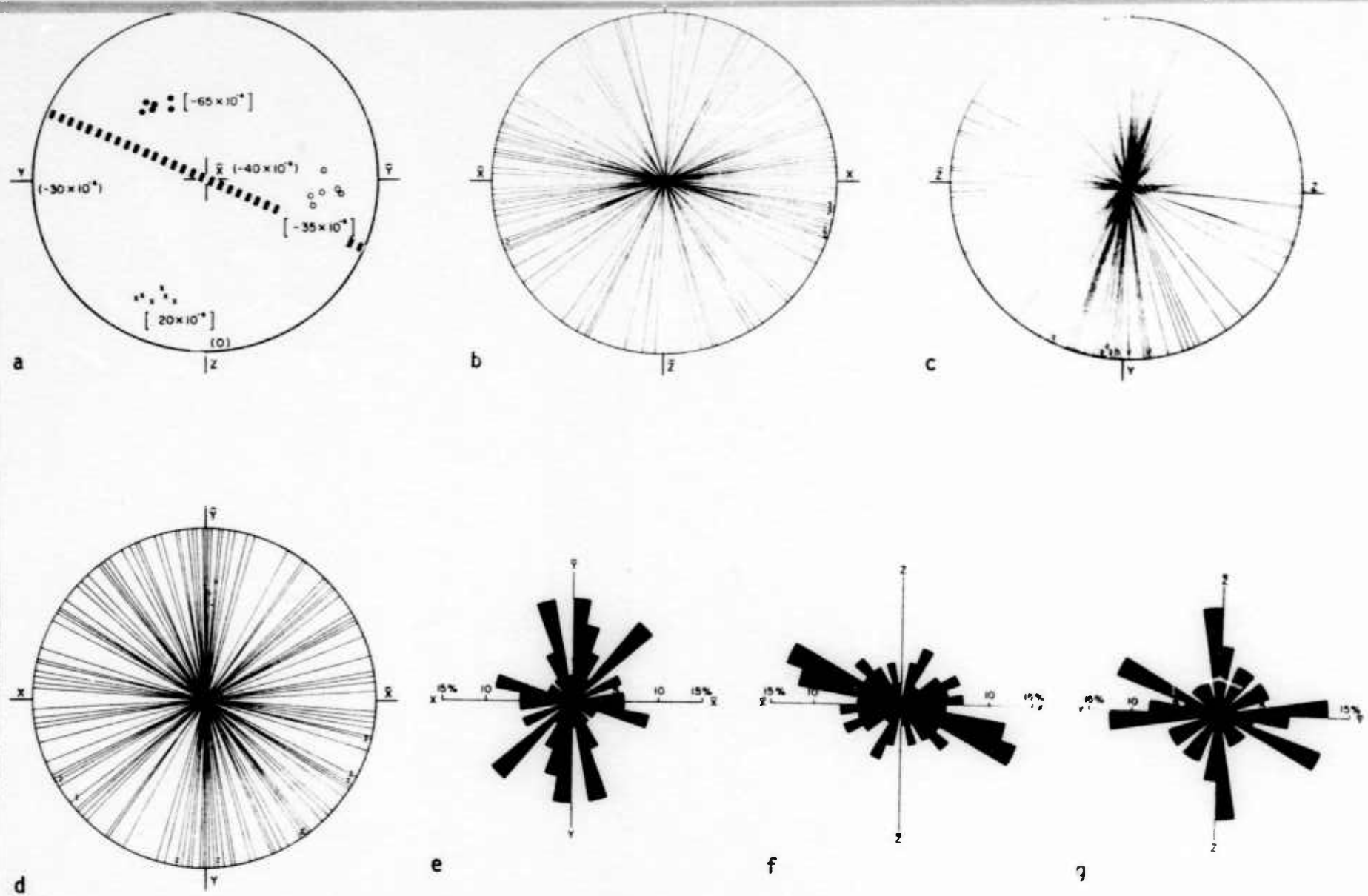

Figure 3. Residual strain, fracture anisotropy, and fabric data for Charcoal Granite. (a) Six sets of residual principal strain axes are plotted in equal area, lower hemisphere projection. X, O, and ● correspond to the greatest, intermediate, and least elongations, respectively. Average strain magnitudes are given for the principal axes and for the directions X, Y, and Z. Dashed line indicates predicted direction of tensile fractures, point loading tests. Diagrams b, c, and d show the orientations of the traces of 51, 58, and 66 tensile fractures induced by point loading parallel to Y, X, and Z, respectively. Diagrams e, f, and g show the angular distribution of 34, 48, and 41 long grain boundaries, respectively.

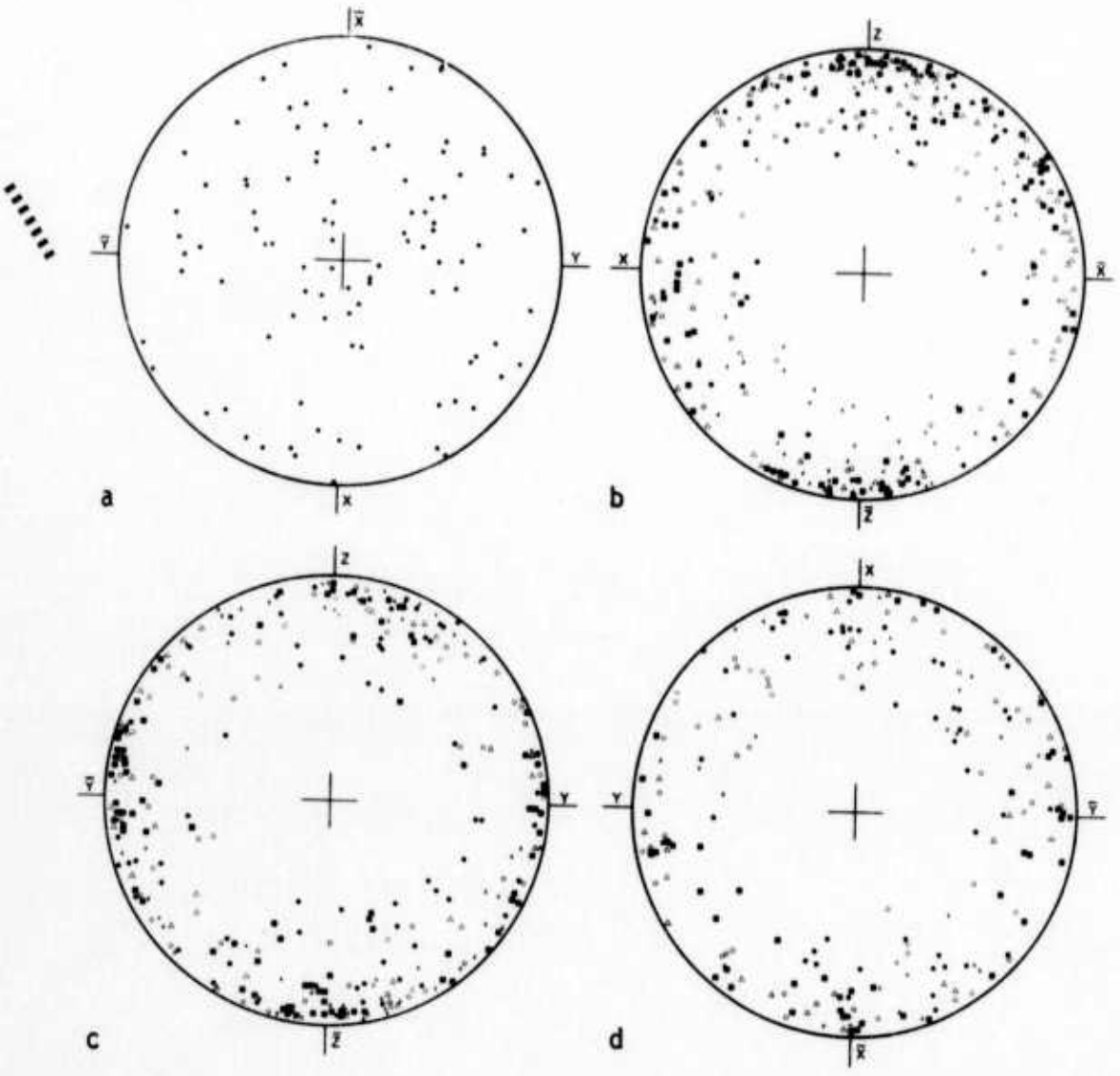

Figure 4. Diagrams show orientation of planar fabric elements in Charcoal Granite. Data are plotted in lower hemisphere, equal area projection. (a) Composite diagram of normals to (0001) cleavages in 100 biotite crystals measured in three mutually perpendicular thin sections. Partial diagrams (b, c, and d) show the orientations of normals to microfractures ■ , feldspar exsolution lamellae X, feldspar (010) cleavages Δ , feldspar albite twin lamellae ●, and microcline twin lamellae 0 as measured in thin section cut parallel to the XZ, YZ, and XY planes, respectively. In (b) the number of data points are 98 ■ , 82X, 64Δ , and 53 ●, and 36 0. In (c) the corresponding numbers are 87, 65, 30, 66, and 55; and in (d) there are 50, 30, 29, 50, and 44 data points, respectively.

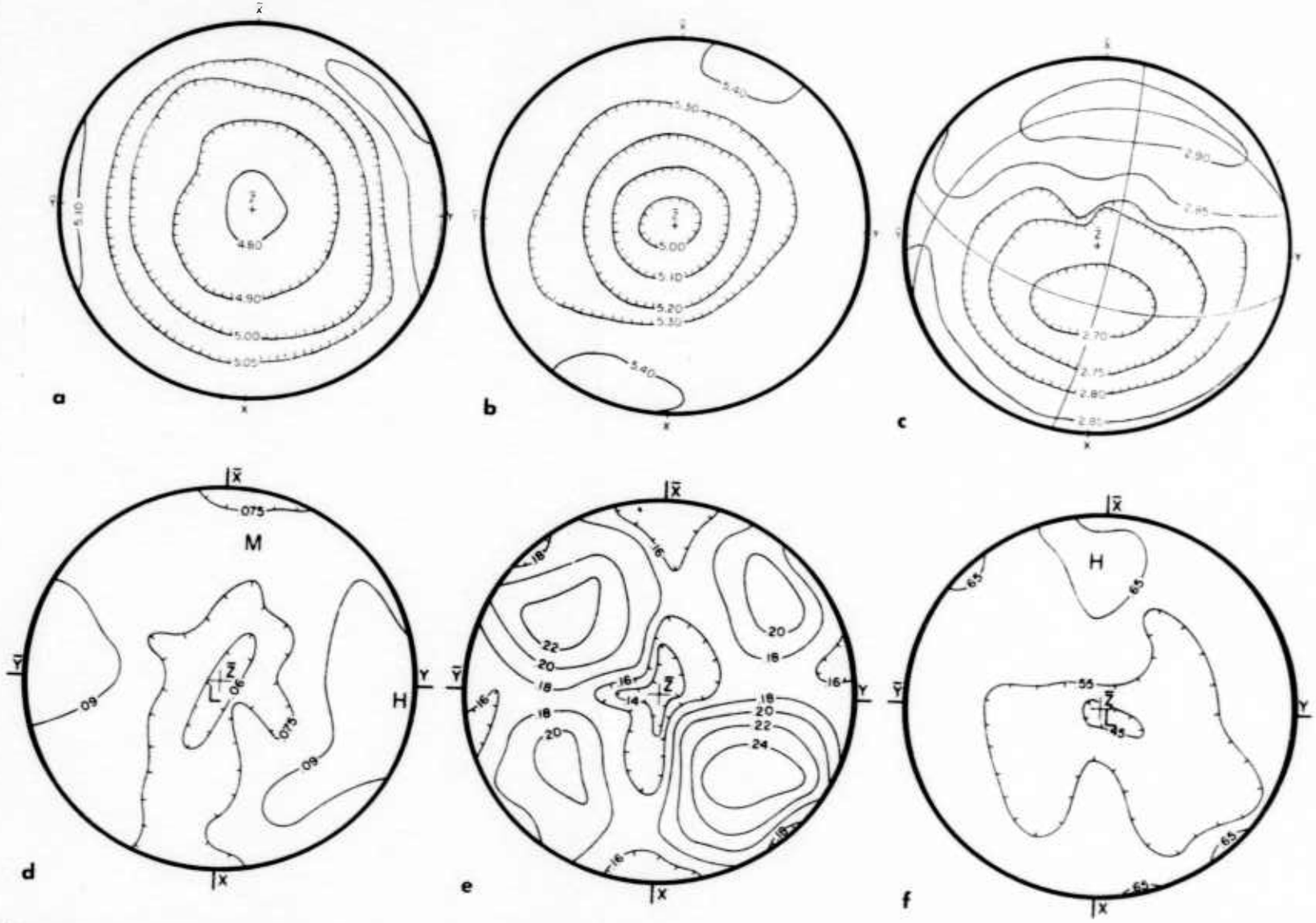

Figure 5. Ultrasonic data for Charcoal Granite (a,d), Sioux Quartzite (b,e) and Berea Sandstone (c,f) supplied by staff of the U.S. Bureau of Mines, Twin Cities Mining Research Center. All data are plotted in equal-area, lower hemisphere projection. Average velocities in km/sec are plotted in a-c; relative amplitudes, the inverse of attenuation, are plotted in d-f.

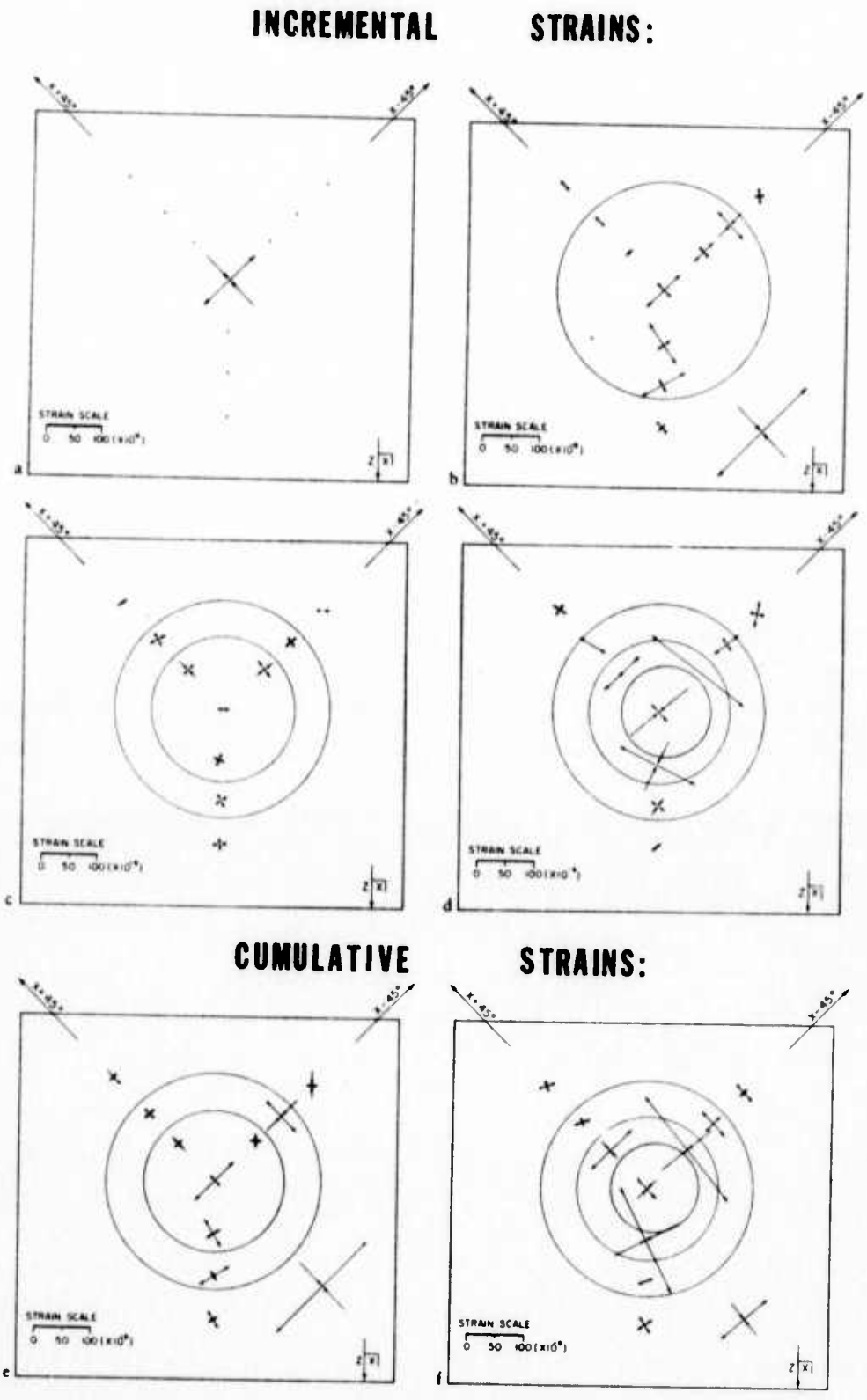

Figure 6. Strain-relief data for Sioux Quartzite. Arrows indicate orientations and relative magnitudes of principal strain changes (i.e., relaxations) in the XY plane of the block. Incremental strains result solely from the test overcore, and the 15-cm, 10-cm, and 5-cm diameter overcores in a, b, c, and d, respectively. Cumulative strains in e and f are summed from "zero" readings established after the test overcore. The principal axes in the lower right corner of b, e, and f are cumulative strains at rosette 1 (Figure 1) including those resulting from the test overcore. X+45° and X-45° are directions mentioned in text.

Sioux Quartzite

After 15-cm overcore:

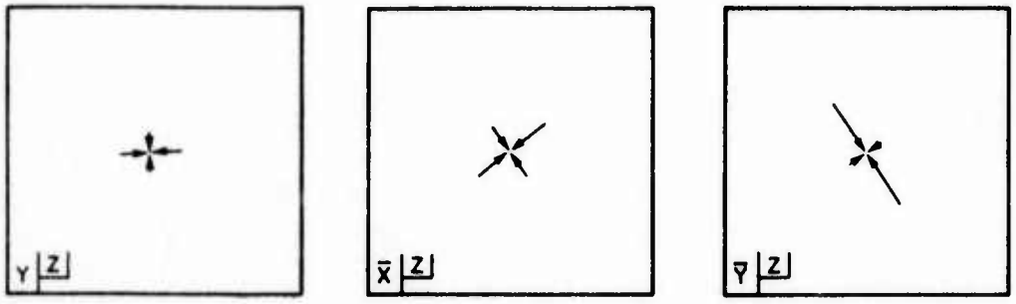

Rosette: 11 12 13

0 25 x 10⁻⁶

After 10-cm overcore:

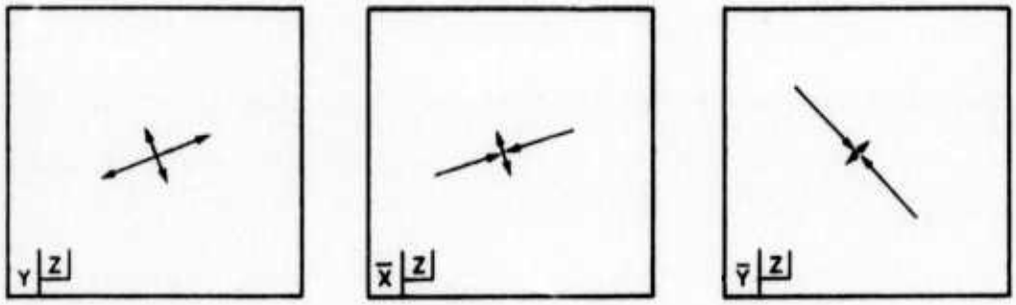

Rosette: 11 12 13

After 5-cm overcore:

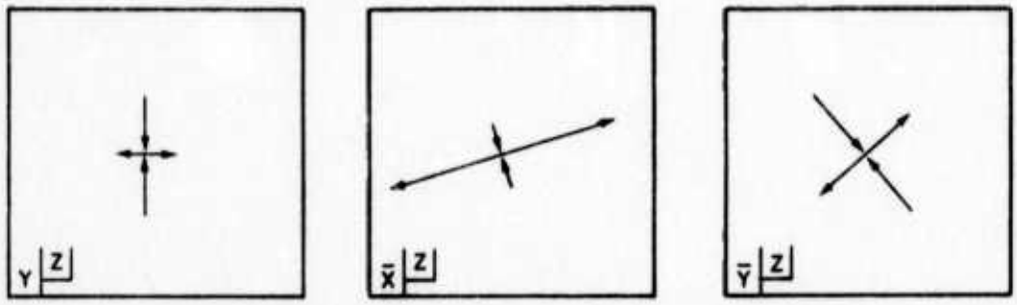

Rosette: 11 12 13

Figure 7. Cumulative principal strains at rosettes 11, 12, and 13, Sioux Quartzite.

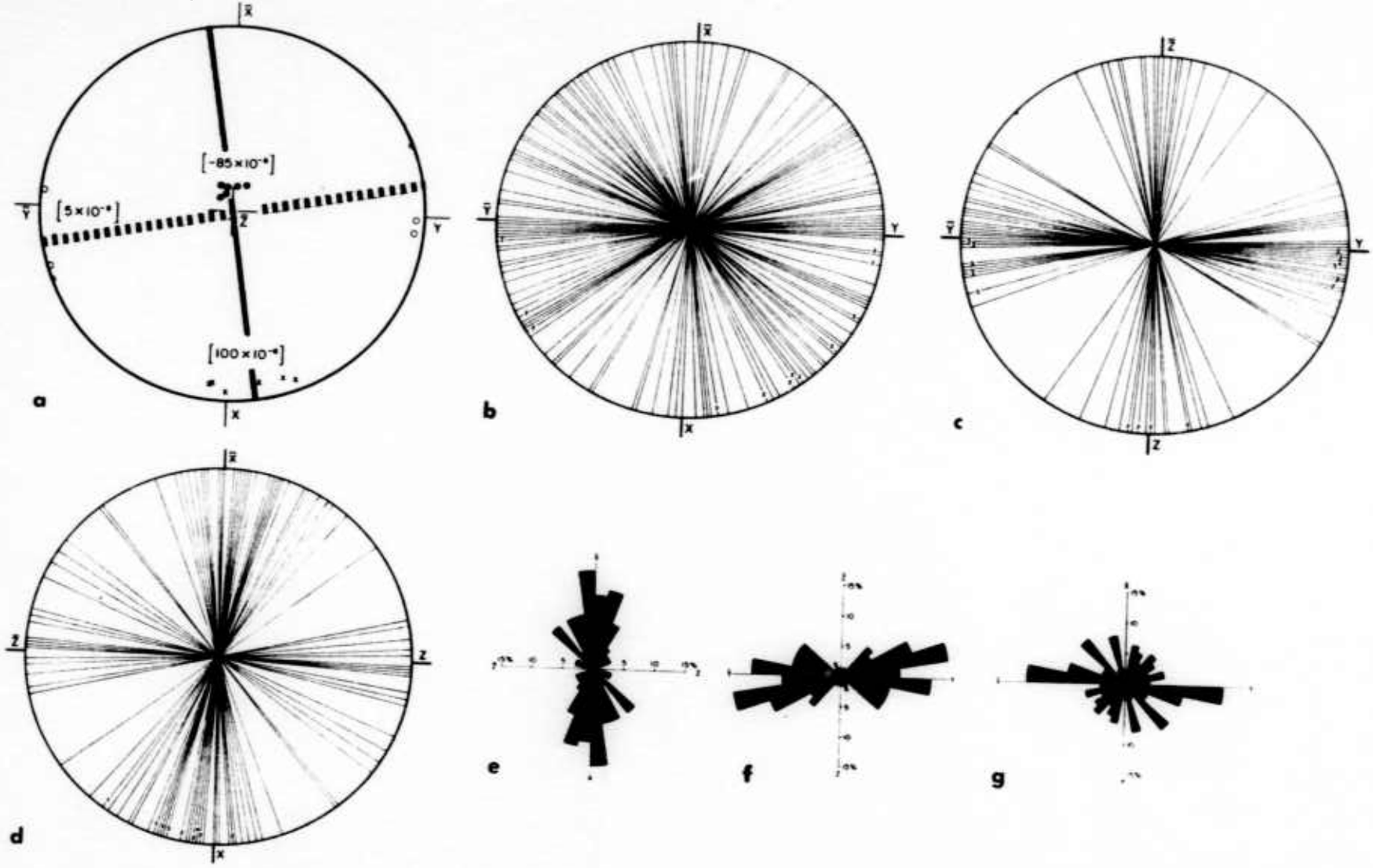

Figure 8. Residual strain, fracture anisotropy, and fabric data for Sioux Quartzite. (a) Six sets of residual principal strain axes are plotted in equal area, lower hemisphere projection. X, O, and ● correspond to the greatest, intermediate, and least elongations, respectively. Average strain magnitudes are given for the principal axes. Dashed line indicates predicted trend of tensile fractures when discs are point loaded parallel to Z. Solid line is the predicted trend when point loaded parallel to X. Diagrams b, c, and d show the orientations of the traces of 80, 66, and 66 tensile fractures induced by point loading parallel to Z, X, and Y, respectively. Diagrams e, f, and g each show the angular distribution of 75 apparent long grain axes.

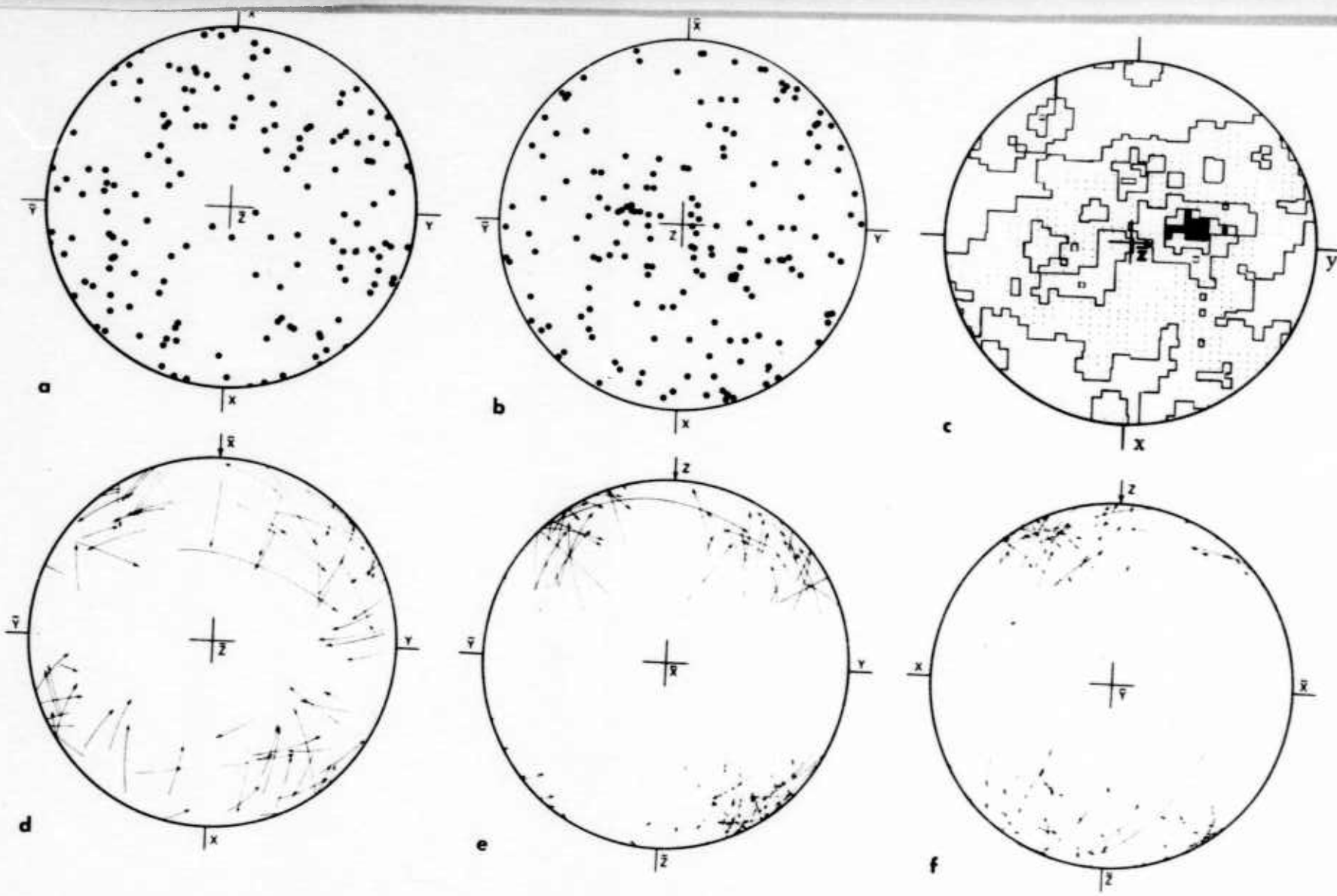

Figure 9. Fabric data for Sioux Quartzite. All data are plotted in equal area, lower hemisphere projection. (a) 150 quartz c-axes. (b) Composite diagram of normals to 170 sets of healed microfractures. (c) Composite diagram of normals to 200 sets of quartz deformation lamellae. Contours are at 0.5, 2.5, 4.0, and 5.0 per 1-percent area, 6-percent maximum. Diagrams (d, e, and f) illustrate orientation of normals to deformation lamellae (points of arrows) and host c-axes (ends of arrows) in 66 quartz grains each. Arrows "point" toward the orientation of σ_3 at the time the lamellae were formed.

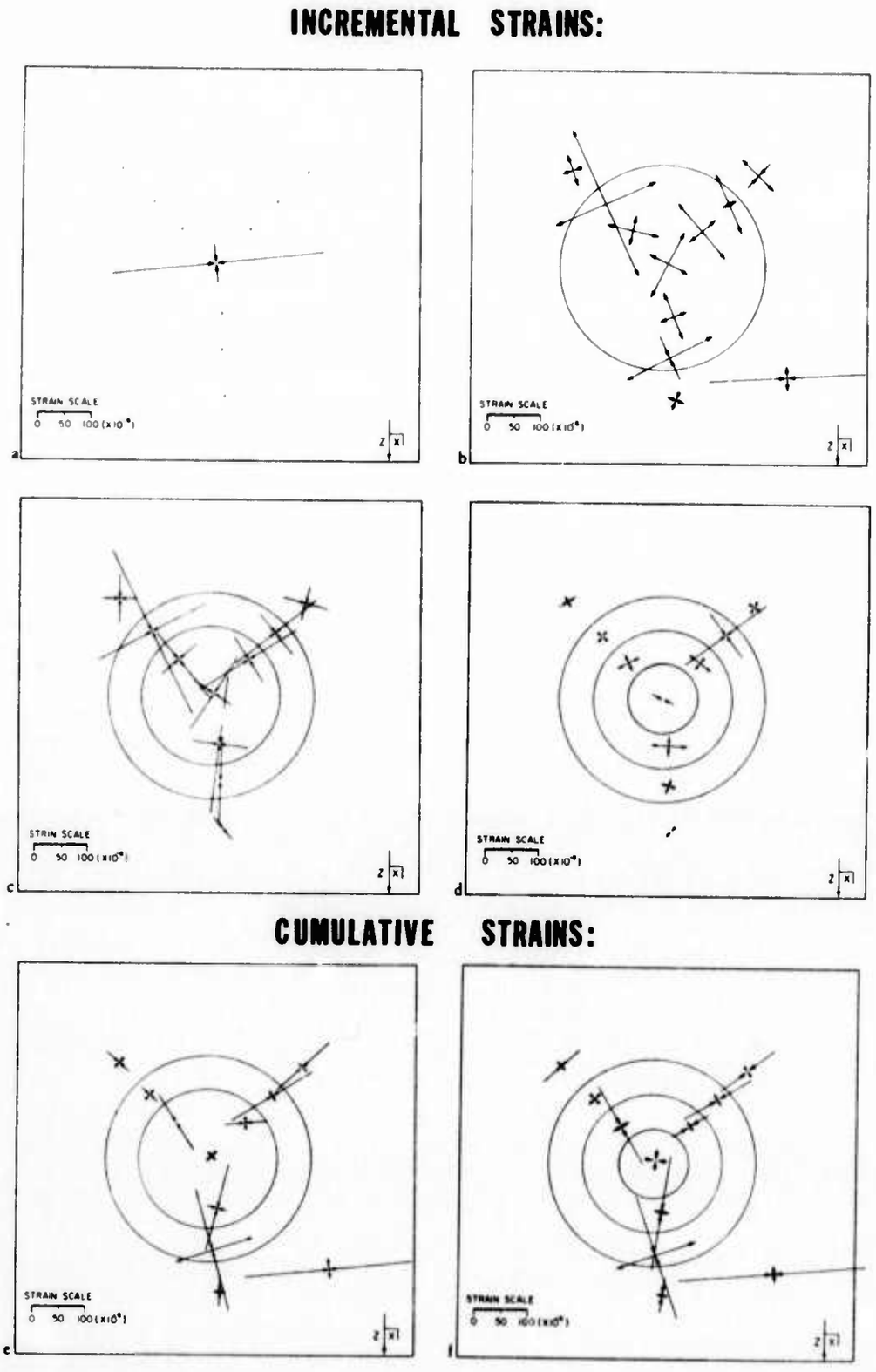

Figure 10. Strain-relief data for Berea Sandstone. For details see caption for Figure 6.

Berea Sandstone

After 15-cm overcore:

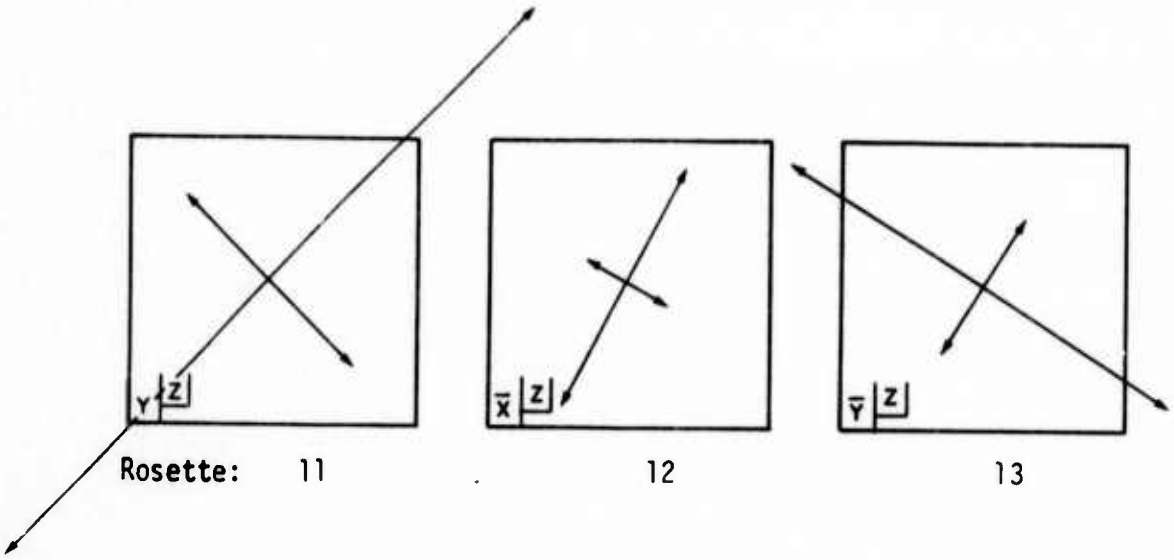

Rosette: 11 12 13

0 50 x 10^{-6}

After 10-cm overcore:

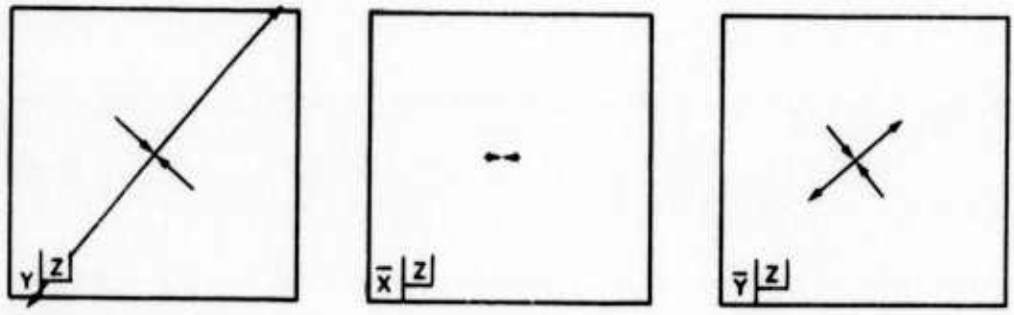

Rosette: 11 12 13

After 5-cm overcore:

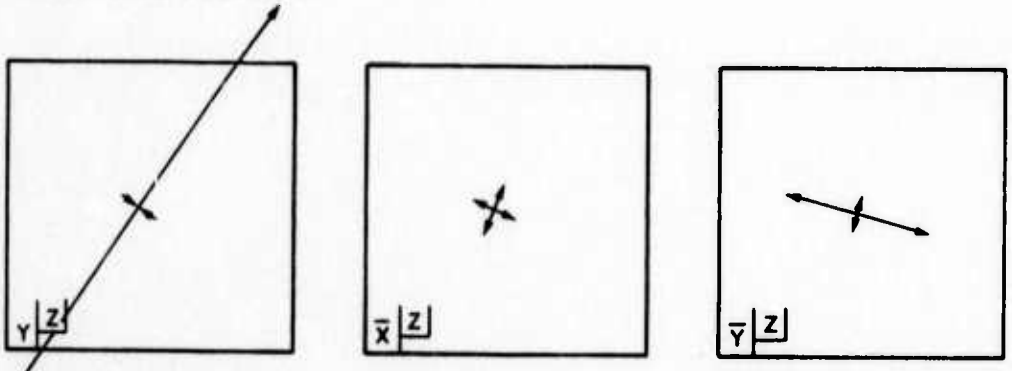

Rosette: 11 12 13

Figure 11. Cumulative principal strains at rosettes 11, 12, and 13, Berea Sandstone.

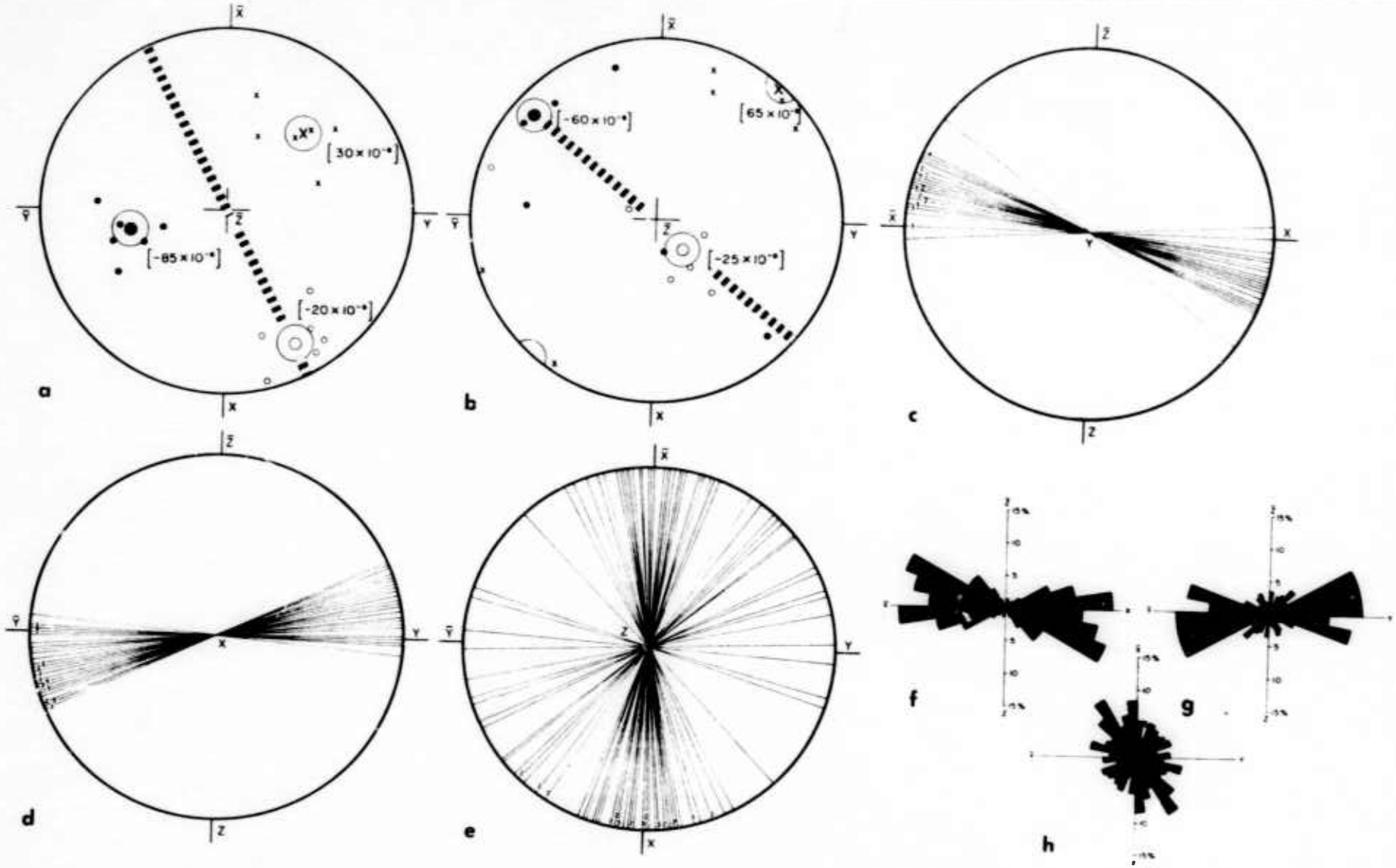

Figure 12. Residual strain, fracture anisotropy, and fabric data for Berea Sandstone. Diagrams a and b each show orientations and average magnitudes of residual principal strain axes plotted in equal area, lower hemisphere projection. Data in (a) comes from the test overcore, that in (b) from under rosette 1. X, O and ● correspond to the greatest, intermediate, and least elongations, respectively. Dashed lines indicate predicted trends of tensile fractures when discs are point loaded parallel to Z. Diagrams c, d, and e show the orientations of the traces of 36, 40, and 66 tensile fractures induced by point loading parallel to Y, X, and Z, respectively. Diagrams f, g, and h each show the angular distribution of 200 apparent long grain axes.

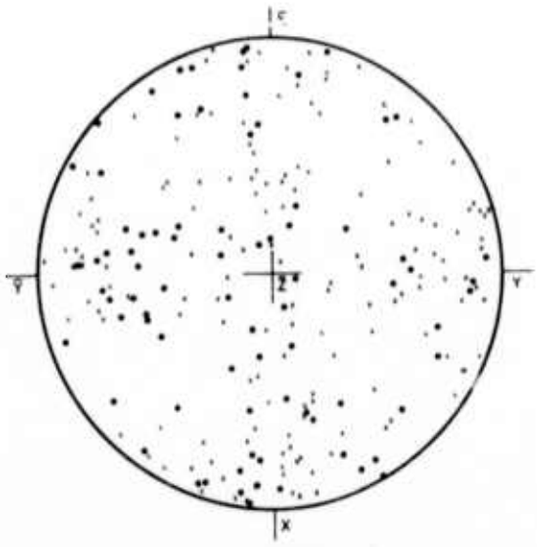

Figure 13. Diagram illustrates orientation of normals to 150 sets of microfractures (X, 2 or more parallel microfractures per set) and 86 sets of quartz deformation lamellae (●). Data are plotted in lower hemisphere, equal-area projection.

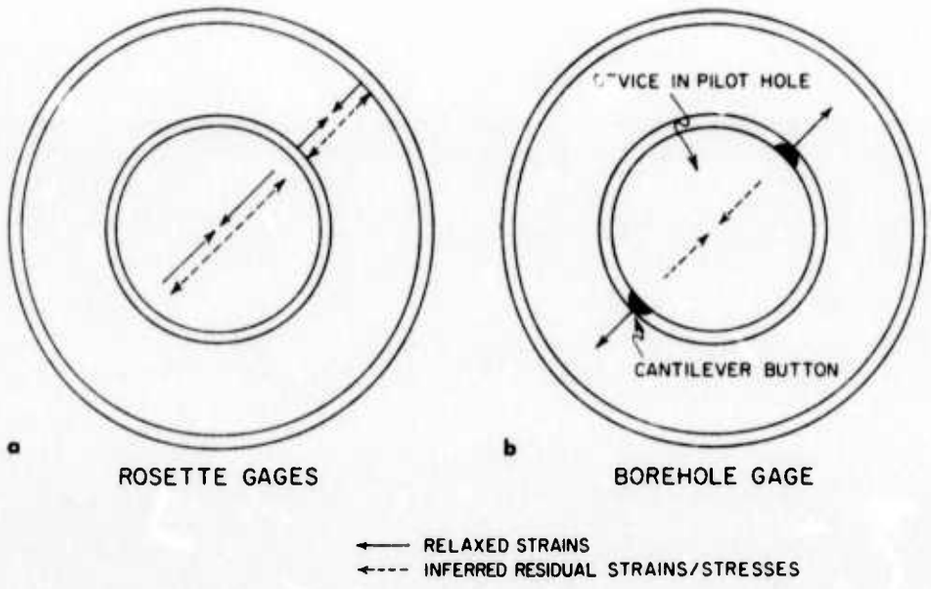

Figure 14. Schematic comparison of inferences drawn from strain-relief data for a rock with residual strain. (a) Nature of relaxation and inferences are shown for strains detected with electric resistance gages (a) and a borehole gage (b).